

AN ABSTRACT OF THESIS OF

Adam Fowler for the degree of Master of Science in Radiation Health Physics

Presented on December 10, 2010.

Title: Skin Depth Dose Response of an Ionization Chamber and a Thermo-luminescent Dosimeter System using Low Energy X-rays.

Abstract approved:

David M. Hamby

The use of Ionization Chambers and Thermo-luminescent dosimeters (TLD's) in the medical field has established a need to determine if the skin depth dose response is comparable between the two detectors. This research will determine if the dose response from an Ionization chamber is comparable to a Thermo-luminescent dosimeter system to improve patient dosimetry. The TLD's to be utilized are the thinnest LiF TLD-100's currently manufactured (0.3175 cm x 0.3175 cm x 0.0152 cm). The TLD's were irradiated with a Radium-226 pin-wheel source to construct the appropriate calibration curve. The calibration curve in turn was used to determine doses to the experimental TLD's for various skin and tissue depths. A Sedecal X Plus X-ray machine was used to determine the dose at certain depths within a Plexiglas phantom material for both the Ionization chamber and TLD's. VARSKIN version 4 computational code and hand calculations were compared to the experimental data.

©Copyright by Adam Fowler

December 10, 2010

All Rights Reserved

Skin Depth Dose Response of an Ionization Chamber and a Thermo-luminescent
Dosimeter System using Low Energy X-Rays

by

Adam Fowler

A THESIS

Submitted to

Oregon State University

in partial fulfillment of

the requirements for the

degree of

Master of Science

Presented December 10, 2010

Commencement June 2011

Master of Science thesis of Adam Fowler

presented on December 10, 2010.

APPROVED:

Major Professor, representing Radiation Health Physics

Head of the Department of Nuclear Engineering and Radiation Health Physics

Dean of the Graduate School

I understand that my thesis will become part of the permanent collection of Oregon State University libraries. My signature below authorizes release of my thesis to any reader upon request.

Adam Fowler, Author

ACKNOWLEDGEMENTS

I would like to thank Marjorie Slauson for all the input and help she graciously provided throughout my thesis project and the usage of the Ionization Chamber. I would also like to thank Scott Menn for all the help with the TLD's. I would like to thank Stacy Mallory for letting me have access to the x-ray machine at the Lebanon Hospital. I would like to sincerely thank my advisor Dr. David Hamby for his input, guidance, and wisdom. I would also like to thank my friends and family who have always believed in me and have encouraged my academic success. Last but not least, I would like to thank my parents and wife who have always been optimistic about my academic endeavors and have pushed me to succeed.

TABLE OF CONTENTS

	<u>Page</u>
1.0 INTRODUCTION	1
2.0 BACKGROUND INFORMATION	3
2.1 SKIN AND TISSUE BIOLOGY	3
2.2 LITERATURE REVIEW	5
2.3 REGULATIONS	7
2.4 X-RAY MACHINE AND PRODUCTION	9
2.5 THEORY	11
2.5.1 X-Ray Interactions	11
2.5.2 Dose and Equivalent Dose	15
2.5.3 KERMA	15
2.5.4 Exposure	15
2.5.5 Charged Particle Equilibrium	16
2.6 THERMOLUMINESCENT DOSIMETERS	17
2.7 TLD READER	20
2.7.1 Photomultiplier Tubes	21
2.7.2 Chip Variability	22
2.7.3 Reader Distribution	23
2.7.4 TLD Fade	23
2.7.5 Fluorescent Light Study	25
2.8 IONIZATION CHAMBER	27
2.9 VARSKIN	38
3.0 TLD EXPERIMENTAL	39
3.0.1 TLD Annealing	39
3.0.2 Processing TLDs	40
3.1.3 Calibration Curves	41
4.0 FACTORS AFFECTING DOSE	44
5.0 EXPERIMENTAL	46
5.1 PHANTOM DESIGN	46
5.2 EXPERIMENTAL PROCEDURE	47
6.0 CALCULATIONS	51
6.1 VARSKIN CALCULATIONS	52

TABLE OF CONTENTS (Continued)

	<u>Page</u>
6.2 HAND CALCULATIONS.....	53
7.0 RESULTS	54
8.0 CONCLUSIONS.....	68
9.0 FUTURE WORK.....	70
10.0 BIBLIOGRAPHY.....	72

LIST OF FIGURES

<u>Figure</u>	<u>Page</u>
Figure 2-1: Skin Layers.....	5
Figure 2-2: Sedecal X-Ray Machine.....	10
Figure 2-3: Photoelectric Effect.....	12
Figure 2-4: Compton Scattering.....	14
Figure 2-5: Charged Particle Equilibrium (CPE).....	16
Figure 2-6: TLD Band Gap.....	18
Figure 2-7: TLD Reader.....	21
Figure 2-8: Photomultiplier Tube.....	22
Figure 2-9: Distribution of “Good” Chips.....	23
Figure 2-10: Fade Study Graph.....	24
Figure 2-11: Fluorescent Light Study Graph.....	26
Figure 2-12: Charge Transfer.....	29
Figure 2-13: Electron Attachment.....	30
Figure 2-14: Recombination.....	30
Figure 2-15: Ionization Current.....	31

LIST OF FIGURES (Continued)

<u>Figure</u>	<u>Page</u>
Figure 2-16: Guard Rings and Insulators	33
Figure 2-17: Measuring Circuit of Ion Chamber	34
Figure 2-18: Electrometer	35
Figure 2-19: Compensation.....	36
Figure 2-20: Ion Chamber	38
Figure 3-1: TLD Glow Curve	40
Figure 3-2: Low Dose Calibration Curve.....	43
Figure 3-3: High Dose Calibration Curve.....	43
Figure 5-1: Phantom Design	46
Figure 5-2: X-Ray Machine Tube Height	49
Figure 5-3: Surface Dose with Ion Chamber	50
Figure 5-4: Exit Dose with Ion Chamber	51
Figure 6-1: Linear Interpolation Graph.....	52
Figure 7-1: Skin Dose Comparison Between Ion Chamber and TLD	57
Figure 7-2: Tissue Dose Comparison Between Ion Chamber and TLD	57

LIST OF FIGURES (Continued)

<u>Figure</u>	<u>Page</u>
Figure 7-3: Dose Comparison Between Ion Chamber and TLD.....	58
Figure 7-4: Varskin, Ion Chamber, and TLD Dose Comparison (0.01524 cm ²).....	59
Figure 7-5: Varskin, Ion Chamber, and TLD Dose Comparison (2.5 cm ²).....	59
Figure 7-6: Varskin, Ion Chamber, and TLD Dose Comparison (10 cm ²).....	60
Figure 7-7: Dose Comparison Between Hand Calculations and Ion Chamber.....	65
Figure 7-8: Dose Comparison Between Hand Calculations and TLD.....	66

LIST OF TABLES

<u>Table</u>	<u>Page</u>
Table 2-1: Fade Study Data	25
Table 2-2: Fluorescent Light Study Data	27
Table 3-1: Exposure Time for TLD Calibration	42
Table 7-1: TLD Readout	54
Table 7-2: Ion Chamber Dose	55
Table 7-3: Percent Difference of TLD and Ion Chamber	56
Table 7-4: Varskin, Ion Chamber and TLD Dose Comparison (.01524 cm ²)	61
Table 7-5: Varskin, Ion Chamber and TLD Dose Comparison (2.5 cm ²)	62
Table 7-6: Varskin, Ion Chamber and TLD Dose Comparison (10 cm ²)	63
Table 7-7: Percent Difference of Ion Chamber and Hand Calculations	67
Table 7-8: Percent Difference of TLD and Hand Calculations.....	68

1.0 Introduction

This research serves to compare the skin depth dose response of an ionization chamber with the response of a Thermo-luminescent dosimeter (TLD) system. With this comparison, it is hoped that the ionization chamber, used for calibration, can be shown to perform dose evaluations similar to TLDs and thus improve our confidence in patient dosimetry.

Ionization chambers are often used for calibration of x-ray machines. The calibration testing that this research is interested in is the surface dose measurements performed with an ionization chamber. Quality Assurance testing on an x-ray machine is designed to simulate standard x-ray procedures and to allow the physicist to check the x-ray beam characteristics for inconsistencies. For example, this experiment was designed to the specifications of an AP (anterior-posterior) abdominal x-ray procedure. If the x-ray machine is not calibrated correctly and the regular quality assurance has not been performed, an over-exposure to the patient could occur which means more dose to patient than necessary.

Thermo-luminescent dosimeters, used in this context, monitor patient's when a standard x-ray procedure is performed. The TLD is taped to the skin of the patient in the x-ray area to measure a surface dose. The surface dose can be compared to national standards to see if the dose is in range for that specific type of procedure. The disadvantage to using national standards is that the surface dose from each x-ray machine is different and there is a large variation between dose measurements. By using the calibration testing (surface dose from ion chamber) on a specific x-ray machine, you can correlate the patient dose using TLD's to the calibration dose and monitor both patient dosimetry and calibration testing from the same x-ray machine. Therefore, the dose response of TLD's and an ionization chamber should correspond with each other during calibration testing and during a standard x-ray procedure.

Furthermore, ionization chambers and TLD's must be comparable so physicists have the ability to utilize both detectors during calibration testing for their surface

dose measurements. During a standard x-ray procedure, the diameter of the ionization chamber is too thick to determine an exact surface dose and will be visible on the x-ray image. Thus, TLD's can be used to determine a more accurate surface dose when an x-ray procedure is completed and will not be visible in the x-ray image. The small size of the TLD will make surface dose measurements easier for the physicist because TLD's can be placed on surfaces and their small size and thickness make for a more accurate surface dose. Whereas the ionization chamber relies on a mounting stand to hold it at certain locations in the x-ray field. Two detectors will be utilized which make for more accurate surface dose results and reassurance from two detectors.

The monitoring of patient skin dose must be associated with the surface dose measurements with the ionization chamber. Thus, by designing an experiment which determines the skin depth dose response of each detector within a tissue equivalent phantom (Plexiglas), the correlation of the associated dose response can be determined. The TLD and the ionization chamber dose response will be monitored at different depths within a tissue equivalent phantom to determine if each detector provides an equivalent dose comparison.

The ionization chamber and TLD skin depth dose response will be compared to hand calculations. Hand calculations for absorbed dose (which are calculated from the surface dose) will be compared with the absorbed dose from the ionization chamber and the TLD to determine if they are comparable. During a standard x-ray procedure, the dose is measured on the surface of the skin and the absorbed dose at any depth to the tissue can thus be approximated with the surface dose measurement. The dose can be approximated using a simple calculation with the appropriate transmission factor. The absorbed dose from each detector will be compared to hand calculations.

The TLD and ionization chamber will also be compared to VARSKIN, a program used for assessing doses from skin contamination, including hot particles. The VARSKIN program will take into account the parameters of an x-ray machine and

will be set as close as possible within its programmable limits, since VARSKIN is used for measuring dose from skin contamination and not from an x-ray machine.

2.0 Background Information

2.1 Skin and Tissue Biology

The skin contains various layers with different biological and physical design. The thickness of the skin is of utmost significance for this research because this will determine the skin depth increments and at which depth each dose should be measured. To determine skin depth increments, the biology must be understood so the correct depth increments can be chosen.

The outer most layer of the skin is called the epidermis and forms the waterproof protective layer over the bodies' surface. The epidermis is made of stratified squamous epithelium with an underlying basal lamina. The basal lamina is a layer of extracellular matrix which the epithelium can lay on and which is secreted by the epithelial cells (Martini 2006). The epidermis contains no blood vessels, so cells in the deepest layers are supplied by diffusion of blood capillaries which extend to the upper layers of the dermis. The epidermis can be further divided into 5 different sub-layers or strata which make the diffusion of chemicals and pathogens into the dermis fairly tough. The outermost layer of the epidermis contains 25-30 layers of dead cells. The dead cell layer is referred to as the stratum corneum and is approximately 25 percent of the total epidermis thickness (Martini 2006). The thickness of the stratum corneum can vary depending on the location on the body, such as the palms of the hands or the soles of the feet.

The stratum granulosum is below the stratum corneum and this section or layer of skin consist's of 4 to 5 layers of compressed cells with a degenerating nucleus. The cells of importance are located below the stratum granulosum in two different layers, referred to as the stratum spinosum and the stratum germinativum (also known as the

basal layer). These layers provide the epidermis with structure, yet are very radiosensitive. The effects of radiation-induced damage within the epidermis skin layer will be noticeable in these two regions (ICRP 59). The thickness of the epidermis ranges between 0.05 mm to 1.5 mm depending on the location on the body.

The dermis is the next major layer of the skin. It contains connective tissue which cushions the body from stress and strain. The dermis is tightly bound to the epidermis by a basement membrane and contains many nerve endings that provide the sense of touch and heat (Martini 2006). The dermis also holds many different glands for the skins normal function and blood vessels to nourish the skin with oxygen and waste removal from dead cells (Martini 2006). The dermis contains two main sections, the papillary dermis and the reticular dermis. The papillary dermis is located under the stratum germinativum layer of the epidermis and serves as the metabolically active region of the skin with the main purpose of thermoregulation and supporting the stratum germinativum layer (Martini 2006). The reticular dermis is the primary structural component of the skin and is located under the papillary dermis. The total thickness of the dermis layer ranges from 1 to 4 mm depending upon the location on the body. Regions of the body, such as the back, have thicker dermis layers than the extremities (ICRP 59). The total thickness of the epidermal and dermal layers (which make up the two major skin layers) ranges between 4 to 6 mm depending on the location on the body. This thickness will play a large roll in determining what depth increments will be used for skin dose at various depths.

Figure 2-1 depicts the different layers of the skin

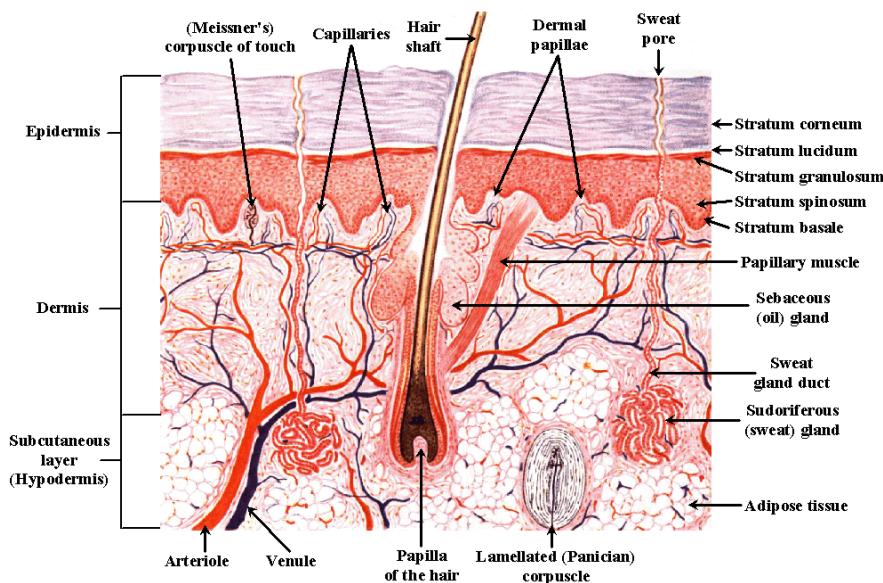


Figure 2-1: Skin Layers (A.D.A.M.)

Radiosensitive skin layers range from 50 μm to 100 μm in the epidermis, which are the basal cells. Regulations monitor a shallow dose at 70 μm (or .007 cm) which is in the range between the radiosensitive skin layers in the epidermis. Deterministic effects are most serious on dermal skin layers ranging from 300 μm to 500 μm .

The tissue which will be of interest is fat tissue since this is the layer below the skin. Since the phantom is designed out of a homogenous material (Plexiglas), it is assumed that this material is fat tissue and will make up the internal structure of the phantom. Fat tissue, or adipose tissue, is loose connective tissue composed of adipocytes, cells which contain fat droplets (Martini 2006). Adipose tissue is mostly made up of water and has an equivalent density to both Plexiglas and water which makes Plexiglas an ideal material for this research.

2.2 Literature Review

The review of the literature has shown that TLD's and ion chambers are comparable with different medical procedures. The literature demonstrates that

research has been performed between the ion chamber and the TLD, but no research has shown the dose response for a standard x-ray procedure.

A study by Stanton (1999) shows the comparison between the ion chamber and the TLD for mammography dosimetry to be comparable for the low energy x-rays used for this procedure. Stanton used a uniform BR 12 “average breast” phantom to compare the ion chamber and the TLD at different depths within the phantom. Stanton found that the ion chamber and TLD dose comparison at each depth was within 5 percent when using the 0.03 mm of Molybdenum and between 4-8 percent when taking the filtration out of the beam.

Kinhikar (2007) performed a study using IMRT (Intensity Modulated Radiotherapy) dosimetry to compare the dose response between the ion chamber, TLD, MOSFET and EDR2 film dosimetric verification for IMRT plans delivered with dynamic multileaf collimators. Kinhikar used a 6MV photon beam to compare the different detectors and found that the Treatment Planning System (TPS) for all detectors was comparable within 5 percent.

Kinhikar (2008) also performed a study using IMRT to compare dose inhomogeneity within a head-and-neck phantom due to hot and cold spots across the phantom to determine the different dose results from an ion chamber, TLD, and Gafchromic film. The measurements carried out between the ion chamber, TLD and Gafchromic film were found to be in good agreements with each.

A study by Hazle (1992) used an ion chamber and TLD's to verify the dosimetry data provided to the Radiation Therapy Chart review office of inter-institutional electron intra-operative radiotherapy. Hazle's results demonstrate that the ion chamber and TLD are comparable both for output and depth dose comparison for intra-operative radiotherapy.

A study by Hobbs (1991) shows the dose comparison between an electret ion chamber and LiF TLD's to be comparable for routine environmental monitoring.

Hobbs placed an ion chamber, TLD's and a HPIC detector at different locations in the grounds of the National Institute for Standards and Technology to determine if the dose comparison is equivalent. Hobbs found that the TLD and ion chamber dose was comparable for routine environmental monitoring.

The literature has proven that the ion chamber and TLD dose response is comparable for different procedures in the radiotherapy field and for environmental monitoring. Thus, an experiment will be designed to determine the dose comparison between the ion chamber and TLD using a standard x-ray procedure.

2.3 Regulations

The International Commission on Radiation Protection (ICRP) provides recommendations for radiation protection internationally. In the United States, the Nuclear Regulatory Commission (NRC) establishes dose limits for radiation workers. The NRC accepted the recommendations set forth by ICRP Publication 59: The Biological Basis for Dose Limitation in the Skin. These regulations are stated in Title 10 of the Code of Federal Regulations Part 20. These regulations are helpful in determining the skin averaging area that must be used for the VARSKIN program and to determine skin dose regulations. The regulations will establish the depth at which skin dose is measured in the United States.

The 10CFR20 states that for occupational workers, the annual limit for shallow dose equivalent is 50 rem averaged over 10 cm² of skin of the whole body or to the skin of any extremity, with a deep dose equivalent of 50 rem. The total annual effective dose equivalent for individual members of the public is 0.1 rem which is the sum of the deep dose equivalent (for external exposure) and the committed effective dose equivalent (for internal exposure). The shallow dose is monitored at a tissue depth of 0.007 cm or 7 mg/cm² and the deep dose equivalent is measured at 1 cm or 1000 mg/cm². Although these parameters are essentially for any exposure to radiation and not for medical exposures, they set a limit for skin and tissue exposure which is

relevant for this research and can be compared to a single exposure from an AP abdominal x-ray procedure.

Furthermore, each state has its own radiological committee which regulates x-ray machines and the dose received by an individual during an x-ray exam. These state agencies ensure that regular Quality Assurance is done on a regular basis so the x-ray machines are delivering the expected dose to the patient. The Food and Drug Administration (FDA) certifies x-ray machines which states that each x-ray machine meets certain performance standards. The Joint Commission on Accreditation of Healthcare Organizations (JCAHO) along with The American College of Radiology (ACR) are examples of agencies which provide guidance for safe x-ray use. The JCAHO and ACR also issue guidance designed to reduce unnecessary use of radiation in diagnosis and treatment to ensure that technicians and equipment meet standards that minimize radiation exposure. The Oregon Radiation Protection Services ensure that x-ray machines are calibrated within the state of Oregon. The radiation safety officer (RSO) and the imaging department manager at each facility work with these agencies to make sure that x-ray exposure is properly regulated and that x-ray machines are properly regulated. The RSO and the imaging department manager are also the overseeing bodies which verify that each x-ray exam is done to the specified procedure outlined and that each patient is not receiving an over-exposure of radiation.

There is no set skin dose limit for medical exposures to radiation for patients. Most guidelines and regulations that are set in the medical field are governed by the “As Low As Reasonably Achievable” (ALARA) concept, translating to the production of a diagnostically relevant image at the minimum possible dose. Consideration should be given to the use of as small a quantity of administered radioactivity as is practical for a diagnostic image.

The reason these limits and regulations are important is because the annual number of medical procedures using ionizing radiation is increasing about 5 to 10% each year

(Health Physics Society 2010). Thus, more procedures are being done which increases the chances of both the patient and the occupational worker to be over-exposed if the Quality Assurance isn't accurately designed. Understanding the comparison between TLD and ion chamber skin depth dose response will allow physicists the ability to more accurately determine the patient dose and will make the calibration testing more precise and reliable.

The entrance dose from an x-ray procedure is the dose received at the body's surface, where the x-ray beam enters. The exit dose, which is what results in an image, is much lower than the surface dose. The body absorbs or scatters the difference between the entrance and exit doses. The surface dose is easily measured during an x-ray procedure; the x-ray technician tapes a small crystal (TLD) to the x-ray area and the crystal responds to the x-ray dose. The crystal does not interfere with the image and easily attaches to the patient's skin. True doses, measured during actual procedures, sometimes differ many-fold from the assumed or calculated doses (Goffman 2000). Unless x-ray practitioners periodically measure the entrance dose and compare them with assumed or calculated doses with calibration testing, practitioners will not know what dose they are really administering (Goffman 2000). The JCAHO requires that x-ray exposures at accredited facilities be measured and compared with national data. By determining if the doses are comparable between the ion chamber and the TLD, physicists will be able to collect this data to meet regulations much easier because they can use both detectors for their calibration testing and for patient monitoring of x-ray surface dose.

2.4 X-ray Machine and Production of X-Rays

The x-ray machine used for this research was a Sedecal X-Plus (Model Number A8117-10) universal radiographic system with a digital detector. The Sedecal X-Plus is designed to give the maximum flexibility and clinic productivity. The x-ray machine has an immense range of possible studies for trauma applications, thorax, urology, abdomen, urgencies, enabling AP/PA, lateral exposures on a rod-able table

(Sedecal 2010). The Sedecal X-Plus system contains a high frequency x-ray generator with flat panel technology for direct digital acquisition. The machine is designed to give a user friendly operating system and easy positioning of the patient (Sedecal 2010). The easy positioning is due to the fully motorized system with variable source to image distance (SID) and anti-collision monitoring. The x-ray system is a perfect application for an antero-posterior abdomen x-ray procedure and utilizes the ease of variable source to image distances and table positioning. The motorized table makes the target SID very easy to position. The machine contains built in laser cross-hares and a light guided collimation system, which makes any patient position very easy to accomplish. The easy design of the Sedecal x-ray machine made setting up the experiment effortless and positioning the phantom within the collimators and in the correct location was not difficult. Figure 2-2 depicts the X-ray machine and the phantom.



Figure 2-2: Sedecal X-Ray Machine

The key component of an x-ray machine is the x-ray tube which produces bremsstrahlung and characteristic x-rays as high-speed electrons interact in the target. High speed electrons originate in a wire filament that is heated by passing an electrical

current to release electrons within the x-ray tube (Hendee 2002). The liberated electrons from the wire filament are repelled by the negative charge of the filament (cathode) and accelerated toward a positive target (anode) within a vacuum. A vacuum is maintained inside the glass envelope of an x-ray tube to prevent electrons from interacting with air molecules within the tube. The x-rays emerge from the target in all directions but, are restricted by collimators to form a useful beam of x rays (Hendee 2002).

The useful beam of an x-ray tube is composed of photons with an energy distribution that depends on four main factors: (1) Bremsstrahlung x rays are produced with a range of energies even if electrons of a single energy bombard the target, (2) x-rays released as characteristic radiation have energies independent of that of the bombarding electrons so long as the energy of the bombarding electrons exceeds the threshold energy for characteristic x-ray emission, (3) The energy of the bombarding electrons varies with the tube voltage, which fluctuates rapidly in some x-ray tubes, (4) x-rays produced at a range of depths in the target of the x-ray tube and will travel through different thicknesses of the target and must penetrate a glass enclosure and may lose energy through one or more interactions (Hendee 2002).

2.5 Theory

2.5.1 X-Rays Interactions

There are three main interactions that an x-ray will undergo when entering a detection medium (human or detector). These interactions include photoelectric effect, Compton scattering, and Coherent scattering. Since x-ray photons are uncharged, incident x-rays need to undergo either photoelectric effect or Compton scattering in order to transfer energy. When an x-ray enters a detection medium, it can either interact by one of the three methods or it can completely penetrate the medium with no interactions occurring.

Photoelectric absorption is a process in which a photon undergoes an interaction with an absorber atom and the photon completely disappears and deposits all of its

energy (Knoll 2000). The photon is replaced by an energetic photoelectron which is ejected by the atom from one of its bound shells and takes away all of the photon's energy less the binding energy. Figure 2-3 depicts the photoelectric effect of an incoming photon.

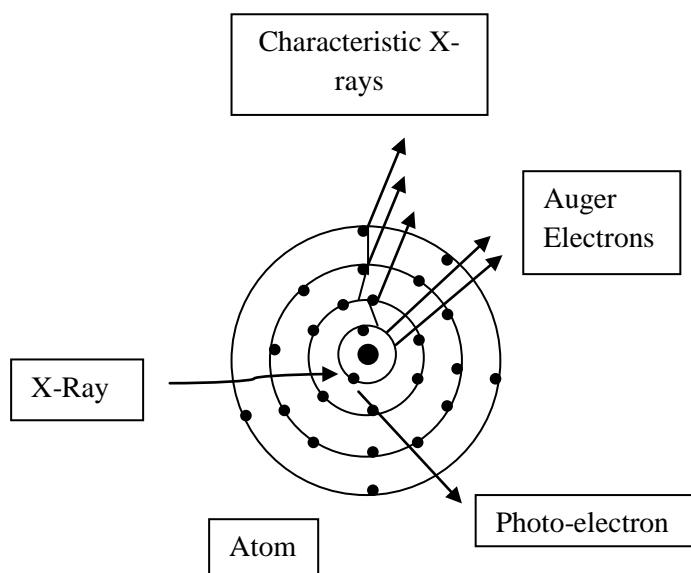


Figure 2-3: Photoelectric Effect (Adapted from Knoll 2000)

The Photoelectric effect interaction occurs with the electrons of an absorber atom as a whole and cannot take place with free electrons in the medium (Knoll 2000). The photoelectron which is produced in the interaction will most likely come from the K shell of the atom, or the most tightly bound shell. This photoelectron will have the energy of the incoming photon minus the binding energy of the photoelectron in its original shell (Knoll 2000). Therefore, the photoelectron carries off the majority of the original photon energy. The electron will rapidly lose its energy and will move only a relatively short distance from its original location. The photon's energy will therefore be deposited in the matter close to the site of the photoelectric interaction. Photoelectric interactions are most probable when the electron binding energy is only slightly less than the energy of the photon. Thus, if the binding energy is more than the

energy of the photon, a photoelectric interaction cannot occur. This interaction is possible only when the photon has sufficient energy to overcome the binding energy and remove the electron from the atom.

The photoelectric absorption interaction also creates an ionized absorber atom with a vacancy in one of its bound shells (Knoll 2000). The vacancy will be filled very rapidly through the capture of a free electron from the medium or rearrangement of electrons from other shells of the atom (Knoll 2000). A characteristic x-ray photon may be generated or an auger electron may substitute and carry away some of the atomic excitation energy. The energy of the characteristic radiation depends on the binding energy of the electrons involved. Photoelectric absorption is the predominant interaction at low x-ray energies and is enhanced as the absorber materials of high atomic number Z are employed.

Compton scattering is an interaction that takes place between the incident x-ray photon and an electron in the absorbing material. This type of interaction is most predominant for x-rays of intermediate energy. In Compton scattering, the incoming x-ray photon is deflected through an angle, θ , with respect to its original direction (Knoll 2000). The x-ray photon transfers a portion of its energy to the electron, which is assumed to be initially at rest, and is called a recoil electron.

Figure 2-4 depicts Compton Scattering of an incoming x-ray.

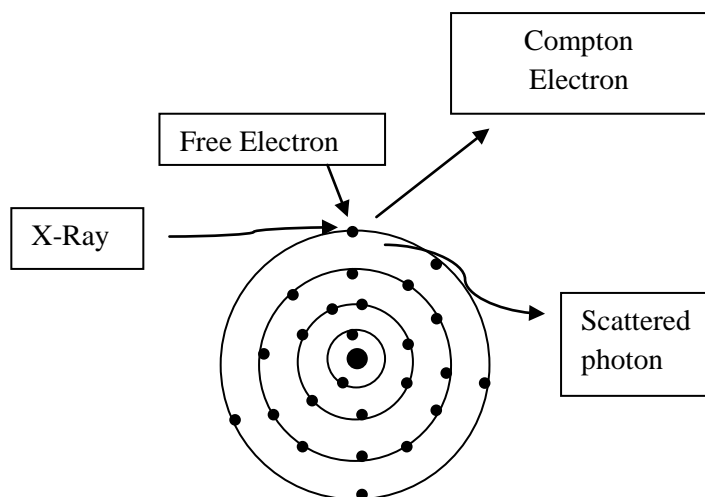


Figure 2-4: Compton Scattering (Adapted from Knoll 2000)

Since all angles of scattering are possible, the energy transferred to the electron can vary from zero to a large fraction of the x-ray energy. When a small scattering angle is produced, very little energy is transferred and the original x-ray photon retains the energy, while the electron takes a small amount of energy in the interaction. The incident x-ray photon will always retain most of the original energy even if the angle is very small. The probability of Compton scattering per atom of the absorber depends on the number of electrons available as scattering targets and therefore increases linearly with atomic number Z (Knoll 2000).

A third type of interaction which occurs in the absorbing material of an incident x-ray is coherent scattering. In coherent scattering, the x-ray interacts coherently with all the electrons of an absorber atom and the scattering neither excites nor ionizes the atom and the x-ray retains its original energy after the scattering events. Since no energy is transferred in the collisions, this process is not as important as photoelectric effect or Compton scattering. For x-rays, the coherent scattering does change the direction of the x-ray, which affects the type of interaction it may undergo. The probability of coherent scattering is significant only for low energy x-rays (below a few hundred keV for common interactions) and is most prominent in high Z absorbers.

2.5.2 Dose and Equivalent Dose

The definition of radiation absorbed dose is energy absorbed per unit mass of material. Radiation dose is measured in units of rad (radiation absorbed dose), which is defined as 100 ergs per gram, where 1 Joule is equivalent to 10^{17} ergs (Cember 2009). The SI unit for dose is the Gray (Gy) and is defined as 1 Joule per kilogram. The rad and the gray are related in that 1 Gray is equal to 100 rads. For x-rays, one rem is equivalent to one rad, so the conversion is very simple.

Equivalent dose is defined as the product of absorbed dose and a radiation weighting factor. The radiation weighting factor for x-ray photons is assigned the value of unity (1). Effective dose is defined as the product of absorbed dose, the radiation weighting factor, and a tissue weighting. Effective dose accounts for individual organs radio-sensitivity. The tissue weighting factors vary for each organ and are based on stochastic risk, for the development of cancer. Tissue weighting factors and the radiation weighting factors are compiled by the ICRP and can vary between ICRP publications as more data on radiation risk is obtained. The current tissue weighting factor stated in ICRP Publication 60 for skin is 0.01.

2.5.3 KERMA

KERMA is defined as kinetic energy released in matter and is the measure of energy transferred from uncharged particles including x-rays, gamma rays, and fast neutrons to ionizing particles per unit mass (Cember 2009). KERMA has the same units as absorbed dose. For KERMA, the mass energy absorption coefficient is equal to μ_{tr}/ρ , and for dose the mass energy absorption coefficient is equal to μ_{en}/ρ .

2.5.4 Exposure

Exposure is a measure of the amount of energy transferred from the x-ray field to a unit mass of air (Cember 2009). One exposure unit is defined as the quantity of x-ray or gamma radiation that produces, in air, ions carrying 1 Coulomb of charge per kilogram of air. The SI unit for exposure is called the roentgen (R). The ion chamber

reads the amount of exposure in millirem which is incident within the chamber volume. Exposure then can be converted to absorbed dose to get a dose measurement.

2.5.5 Charged-Particle Equilibrium (CPE)

Charged-Particle equilibrium (CPE) exists when for a small incremental volume about a given location if for every charged particle leaving the volume, another of the same type and with the same kinetic energy enters the volume traveling in the same direction (Shultis 2002). Figure 2-5 is a depiction of the relationship between KERMA and dose with depth in a given medium.

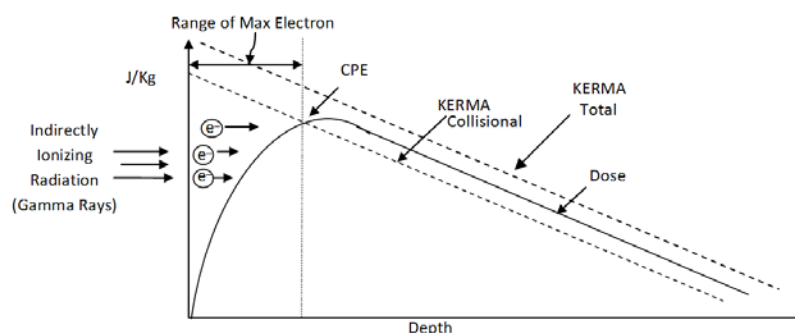


Figure 2-5: Charged Particle Equilibrium

As described in the figure, photons are entering a medium and one of the three interactions (photoelectric absorption, Compton scattering, or Coherent Scattering) with electrons is taking place immediately. KERMA is related to the fluence of the x-ray photon and the attenuation within the medium reduces the fluence exponentially. When the photon interactions produce electrons near the surface of the medium, this is the main contribution to dose at the surface. The dose will see a build up region at the surface as KERMA is producing more electrons, until the depth is equivalent to the maximum range of the electron. At the point where the maximum range of electrons has been met, charged particle equilibrium exists in the medium and the dose and KERMA are equal.

Different material densities will affect the KERMA rate as well as the electron stopping powers of the medium. The effective Z will also have an effect on the KERMA rate. The effective Z for the LiF TLD is 8.2, which is fairly close to the value for tissue of 7.51. We can assume that the LiF TLD is near tissue-equivalent and that CPE is not fully established between the TLD chip and the tissue-equivalent Plexiglas. If the TLD in question was not tissue equivalent, when CPE changes at interfaces between the Plexiglas and the TLD, the x-ray photon will interact with the TLD and another build-up region would take place and further electron interactions would occur.

2.6 Thermoluminescent dosimeters

TLD's work on the basic principle of trapping electrons moving from the valence to the conduction band in various trapping centers between the two band gaps (Knoll 2000). The incident radiation hitting the thermo-luminescent material excites electrons in the valence band toward the conduction band. The excited electrons make it to the conduction band but fall down toward the valence band and get trapped in the forbidden zone from impurities within the crystalline structure. The crystalline structure is between the two bands and serves as electron trapping centers. Therefore, the thermo-luminescent material exposed to a continuous source of radiation leads to the progressive buildup of trapped electrons. The trapped electrons are essentially storing information regarding the radiation energy flux incident on the crystal. The thermo-luminescent material will thus function as an integrating detector in which the number of trapped electrons is a measure of the radiation exposure to the material.

Figure 2-6 depicts the band gap within a TLD crystal.

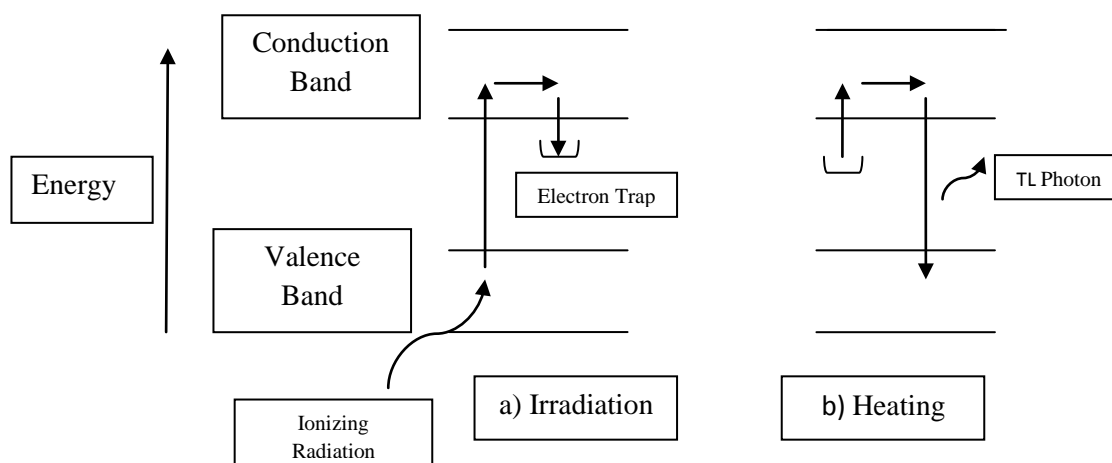


Figure 2-6: TLD Band Gap (Adapted from Khan 2003)

After the TLD is exposed to ionizing radiation, the trapped carriers can be measured through a process in which the material is heated to produce light from the electrons falling from the traps. If the distance of the trap energy level below the conduction band is sufficiently large, there is only a small probability per unit time at ordinary room temperatures that the electron will escape the trap by being thermally excited back to the valence band (Knoll 2000). The TLD sample is placed in a stream of heated gas or on a heated support, and the temperature is progressively raised (Knoll 2000). At a certain temperature, which is determined by the energy level of the trap, the trapped electrons can pick up enough thermal energy so that they are re-excited back to the valence band which is the lower energy state. If the magnitude of the energy difference of the radiated light photon in the band gap is about 3 or 4 eV, the photon is in the visible region and is the basis of the TLD signal. Ideally, one photon will be emitted per trapped carrier and therefore, the total number of emitted photons can be used as an indication of the original number of electrons created by the radiation (Knoll 2000).

TLD's derive a signal by using a heater in which the sample can be viewed by a photomultiplier tube. The light yield is recorded as a function of temperature in a

glow curve in which different TLD material is correlated to calculate the optimum temperature for light output in each material. A glow curve will be constructed from the TLD reader light output and is dependant on the type of TLD material. The integrated glow curve provides information regarding the total amount of trapped electrons (Knoll 2000). The basic signal related to the radiation exposure is the total number of emitted photons, or the area under the glow curve. If the TLD material is exposed to relatively high temperature, all the traps are depleted and the exposure record is lost to light output. Thus, TLD material is very practical in that the material can be reused once it is heated enough to release all of the trapped centers. The TLD reader used in this research provides a single digital output of the summed light output. Newer TLD readout instruments would be required to analyze certain glow curves outputs. In the heating process, electrons fall back to the valence band at a rate of 10^{-8} to 10^{-7} percent per second (Cember 2009).

The TLD's used in this research consist of type TLD-100 from ThermoFisher. The TLD-100's are currently the thinnest chip manufactured and are perfect for measuring skin dose because of their thin design. The thickness of the TLD-100's can be assumed to be negligible because they are so thin. The dose to the thin TLD is very accurate to the surface of the skin and the small thickness can be assumed negligible. The TLD-100's are 0.3175 cm x 0.3175 cm x 0.01524 cm (150 microns). The TLD-100's are made from a natural composition of LiF, with approximately 400 ppm of Magnesium which serves as the primary trapping centers. Thallium is also added with an approximate concentration of 8 ppm which provides luminescent recombination centers during the readout process (Knoll 2000). Thus, the emitted light from the TLD-100 has the characteristic spectrum of the Thallium luminescence site, and re-absorption within the bulk of the material is minimized (Knoll 2000). The light spectrum emitted is a good match for the blue-sensitive photomultiplier tubes used for recording the glow curves of the different material. The natural composition of Lithium contains 92.5 percent ${}^7\text{Li}$ and 7.5 percent ${}^6\text{Li}$. The density of the TLD-100's are 2.64 g/cm^3 and the Z_{eff} is 8.2 which is fairly close to the Z_{eff} for tissue of 7.5. The

TLD-100 trapped charges are very stable at room temperature and their fading rate is very low.

The popularity of the TLD-100 is based on the close match between the atomic numbers of its constituents and those of soft tissue or water. The energy deposited in the LiF is therefore closely correlated with the x-ray exposure or dose equivalent over a wide range of x-ray energies (Knoll 2000). The TLD material can also be reused many times by annealing at elevated temperatures. The downside of TLD material is that there is a great deal of variability between samples and methods of heating. Thus, absolute values of the radiation exposure are normally determined by exposing a source to a known gamma-ray exposure (Knoll 2000). In general, the minimum sensitivity of TLD-100's is about 10^{-2} rads (100 μ Gray), and the signal remains linearly related to dose up to about 400 rads (4 Gy) (Knoll 2000).

2.7 TLD Readers

As mentioned above, the TLD reader works by heating the TLD chip and measuring the light output from the photon emissions via de-excitation of electrons trapped in the crystal's band gap. The TLD to be read is placed on a planchet, which is heated and a temperature is measured through a thermocouple. A thermocouple is a temperature sensor used to control the range of degrees ($^{\circ}$ C) when the heaters temperature is increased. The light photon's that are released from the chip are focused through a filter or wave shifter which converts the emitted photon wave frequency to a visible spectrum which can be collected and read with a photomultiplier tube (PMT). The photomultiplier tube output is then integrated over the specified optimum TLD readout temperatures (100 $^{\circ}$ C to 240 $^{\circ}$ C). The TLD reader used in this research is a Harshaw Model 2000 A/8.

Figure 2-7 depicts a TLD reader and its components.

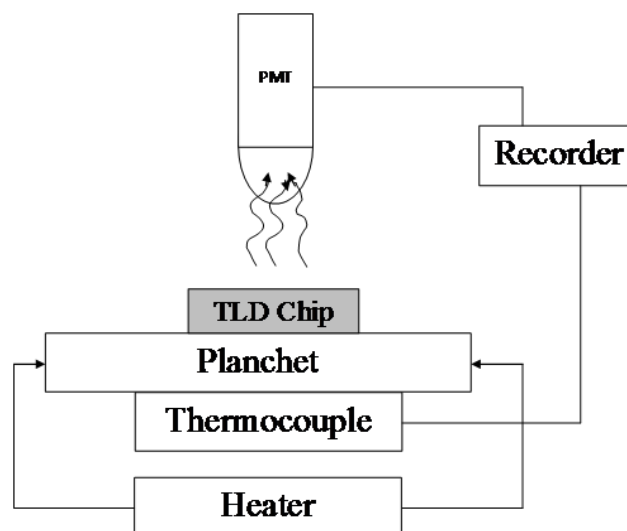


Figure 2-7: TLD Reader (Adapted from Khan 2003)

2.7.1 Photomultiplier Tubes

The photomultiplier tube within the reader is used to convert visible photons emitted from the TLD chip into an electrical signal. The photons liberated from the TLD chip interact with the photocathode. The energy of the incident photon is absorbed into the material and the energy is transferred to an electron. The photocathode serves to convert as many of the incident light photons as possible into low-energy electrons (Knoll 2000). The electrons migrate through the photocathode and are directed toward the electron multiplier. The electron multiplier consists of several dynodes which are designed such that the energy deposited by the incident electron will result in the emission of more than one electron from the surface of the dynode. The electron multiplier section serves to greatly increase or amplify the number of electrons coming from the photocathode. After the multiplication stages, the electrons are collected by an anode and the electrical signal is processed. The photomultiplier tube essentially enhances the signal coming from the TLD chip so there is a readable signal. The number of electrons that are recorded by the anode is

measured in nano-Coulombs. Figure 2-8 illustrates the process of electron multiplication in a photomultiplier tube.

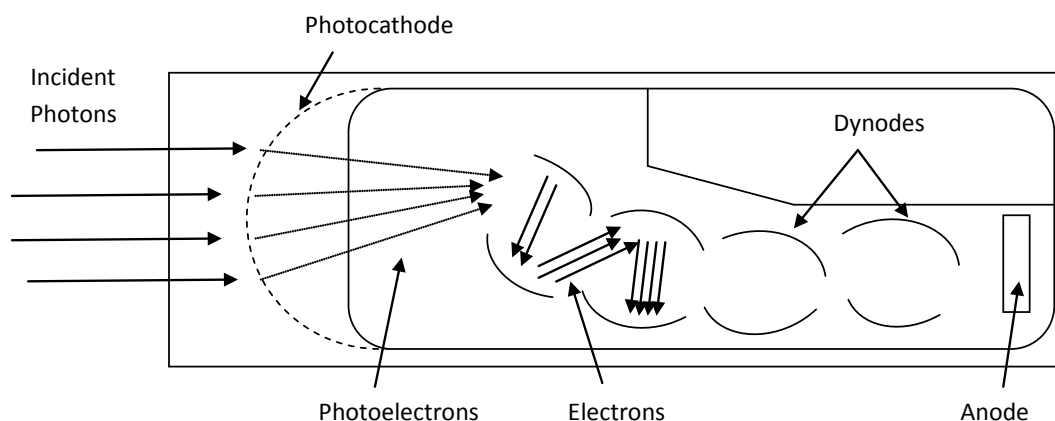


Figure 2-8: Photomultiplier Tube

2.7.2 Chip and Reader Distribution

TLD chips have a great deal of statistical variation between individual chips and even within a given chip. Several chips can be exposed to the same amount of radiation and have varying results. The TLD chips that were selected for this experiment have gone through a quality assurance assessment. The assurance assessment included taking the initially available three hundred chips and exposing them to a 10 μCi Cs-137 button source for a time period of 30 seconds by Krista Keizer (Keizer 2010). The 30 second exposure corresponds to a delivered dose of 0.63 rads to the TLD chip. The chips were readout and the irradiation process was repeated. The chips that read within 25 percent of both irradiations were deemed good chips and were therefore used within this research. For purposes of error propagation, the TLD chip error was assumed to be 25 percent.

Figure 2-9 displays the statistical variations of the good TLD chips.

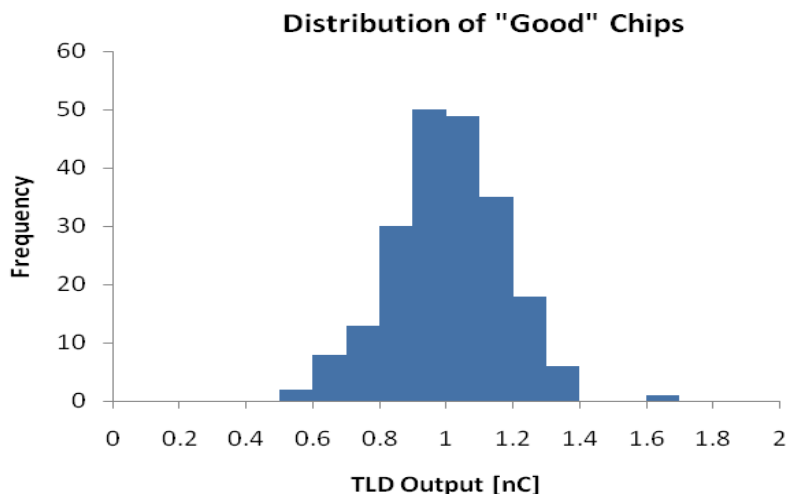


Figure 2-9: Distribution of “Good” Chips

2.7.3 Reader Distribution

The TLD reader also has a statistical variability within itself. The best way to determine if the system is working properly without the influence of the TLD is to take dark current readings. Dark current readings are TLD readings with the drawer completely closed with no TLD chip placed on the planchet and was used for determining operating characteristics of the TLD reader without the influence of a TLD chip. The TLD reader will have some variation in the dark currents when you first begin to use the reader. Once the dark readings have stabilized, the TLD reader is ready to read the experimental TLD’s.

2.7.4 Fade Study

TLD fading is a process in which the trapped electrons within the crystal lattice of the TLD are released before the TLD is read out. If TLD fading is significant, then some of the dose will be lost which will underestimate the correct dose. To determine

if actual fading is significant within this research and to these specific TLDs, a fade study was conducted.

Most of the TLD's within this research were readout within a week of irradiation. The fade time intervals chosen were 1 hr, 1 week, 2 weeks, 3 weeks, and 4 weeks. Most TLDs used for occupational monitoring within the industry have a use time of 1 month and will not be readout until five or six weeks have past. So choosing a fade time interval of 4 weeks is still a viable time interval. A total of 5 TLD chips were used for each time interval to account for statistical variation within the TLD chips. A Radium-226 pin-wheel source was used to irradiate the TLD's with a desired dose of 75 milliRem. The TLD chips were stored in darkness during their assigned fade study period and the temperature did not have much variation. Figure 2-10 displays the TLD fade results with the mean value shown and the standard deviation for the 5 TLD chips.

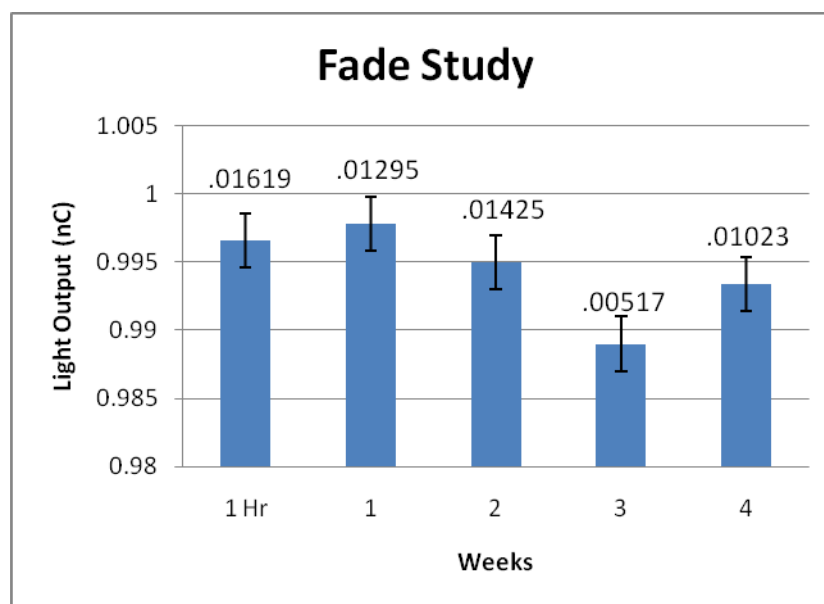


Figure 2-10: TLD Fade

Table 2-1 shows the mean of the 5 TLD chips and the associated standard deviation for each fade time interval.

Ra-222	1 Hr	Week 1	Week 2	Week 3	Week 4
Mean	0.9966	0.9978	0.995	0.989	0.9934
Std Dev (σ)	0.016196	0.01295	0.0142583	0.005177	0.010232
Mean $-\sigma$	0.980404	0.98485	0.9807417	0.983823	0.983168
Mean $+\sigma$	1.012796	1.01075	1.0092583	0.994177	1.003632

Table 2-1: Fade Study

The results of the fade study show that fading is not a factor for the TLD output up to four weeks. The light output at week 4 is within the range of the 1 hour results plus or minus one standard deviation. The results show that the TLD's do not fade over a time period of four weeks.

2.7.5 Fluorescent Light Study

During the research, the TLD's were exposed to a minimal amount of fluorescent lighting which produces UV light and can cause false photon emission when processing the TLD. An irradiated TLD that is exposed to visible light or ultraviolet light may redistribute or lose electrons within the conduction band of the chip (Gad 1991). A study by the International Atomic Energy Agency (IAEA) by (Regulla 1979) showed no significant difference between LiF TLD-100 chips exposed to visible light for an hour to those stored in darkness. There is no literature for LiF TLD-100's exposed to ultraviolet light more than 1 hour, so a fluorescent light study was conducted for up to 24 hours. There is also no literature on ultraviolet light coming solely from fluorescent lights which establishes that a fluorescent light study must be preformed to see if the light is affecting the TLD output.

The lighting within the radiation center and the Lebanon Hospital are produced by fluorescent lighting and very little natural light is let into each facility. Thus, we can

conclude that most of the light is coming from fluorescent lighting and not from natural daylight.

The TLD-100 chips were exposed to a Radium-226 source for 2869 seconds to deliver a dose of 75 mRem to each chip. Five different TLD chips were used for each time interval to account for statistical variation. The time intervals chosen were 1, 3, 6, 12, and 24 hours. The chips were exposed to fluorescent light for the desired time increment and processed. Figure 2-11 displays the results of the fluorescent light study with mean values shown and the standard deviation for the 5 TLD chips.

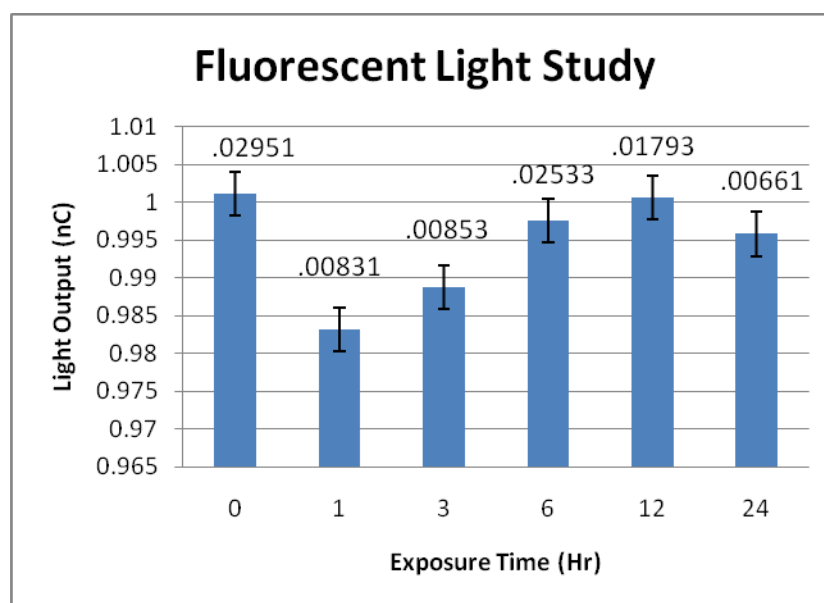


Figure 2-11: Fluorescent Light Study TLD Readout

Table 2-2 displays the average and standard deviation of the five chips at each time interval.

Ra-222	No light	1 Hr	3 Hrs.	6 Hrs.	12 Hrs.	24 hrs.
Mean	1.0011	0.9832	0.98875	0.9976	1.0006	0.9958
Std Dev (σ)	0.029518	0.008319	0.008539	0.025334	0.017939	0.00661
Mean $-\sigma$	0.971582209	0.974881	0.980211	0.972266	0.982661	0.989189
Mean $+\sigma$	1.030617791	0.991519	0.997289	1.022934	1.018539	1.002411

Table 2-2: Fluorescent Light Study Standard Deviation

The results of the fluorescent light study demonstrate that ultraviolet light coming from fluorescent lights have no affect on the TLD output. The time intervals are within the no light standard deviation plus or minus one standard deviation. The 24 hour results are within the range of the no light standard deviation plus or minus one standard deviation. Based on these findings, the TLD-100's are not affected by the exposure of fluorescent light up to 24 hours.

Although these findings show that fluorescent light has no affect on TLD-100's, the utmost care was taken within each procedure of this research to minimize the light exposure to the TLD's. The TLD chips were covered with tin foil when transporting and when storing. The TLD's during the experiment were exposed to fluorescent light for no longer than 1 hour when being x-rayed.

2.8 Ionization Chamber

The Ionization Chamber utilizes the collection of ion pairs when a charged particle passes through a gas to detect the incident radiation. This collection of ion pairs stems from the ionization and excitation of gas molecules along the particles path, hence the name ionization chamber. In principle, the ionization chamber is the simplest of all gas filled detectors and can be constructed very easily because their normal operation is based on collection of charges created by direct ionization within the gas with an applied electric field (Knoll 2000).

Since x-rays are uncharged, they must first interact within the gas medium to deposit all or part of their energy within the medium. The absorption of x-ray energy depends on the type of interaction that occurs within the detector medium. The three main types of interactions for x-rays within a medium include photoelectric absorption, Compton scattering and Coherent scattering. The photoelectric effect or Compton scattering interactions must take place for the x-ray to be detected and deposit its energy within the detection medium since the ionization chamber utilizes charge collection. These interactions are very important for the detection of x-rays and each type of interaction must be understood so there is clear understanding of what is going on inside of the ionization chamber and what energy is being deposited.

X-rays interact through the neutral molecule being ionized within the medium through one of the two interactions, resulting in a positive ion and a free electron which are called an ion pair and serves as the basic constituent of the electrical signal developed by the ionization chamber (Knoll 2000). Ions can be formed either by direct ionization with the incident particle (which occurs through charged particle interactions), or through a secondary process in which the particle energy is first transferred to an energetic electron as in x-ray interactions. Regardless of the mechanisms involved, the ionization chamber is most interested in the total number of ion pairs created along the track of the radiation.

The incoming x-ray must transfer an amount of energy equal to the ionization energy of the gas molecule to permit the ionization process to occur (Knoll 2000). For most gases within an ionization chamber, the ionization energy for the least tightly bound electron shell is between 10 and 25 eV. The average energy lost by the incident particle per ion pair formed (called the W-value) is always substantially greater than the ionization energy so the formation of ion pairs is permitted. The W-value is always defined by three features of the incident radiation: the type of radiation, the type of gas involved, and the energy of the radiation. A typical W-value is between

25-35 eV/ion pair, which means that a 1 MeV particle, if it is fully stopped within the gas, will create about 30,000 ion pairs.

The types of collisions that free electrons, ions, and neutral gas molecules undergo is another important factor in understanding the behavior of gas filled ionization chambers. There are three types of collisions within the detection medium which are an important aspect to the number of ion pairs formed within the ionization chamber including: charge transfer, electron attachment, and recombination.

Charge transfer collisions can occur when a positive ion encounters another neutral molecule within the gas medium. In this type of collision, a positive ion is transferred to a neutral molecule, thereby reversing the roles of each (Knoll 2000). A neutral ion also may be transferred to a positive ion in the same manner. Charge transfer is significant in gas mixtures containing several different molecular species. The transfer is most readily observed when the net positive charge is transferred to the gas with the lowest ionization energy because energy is liberated in collisions which leave the species as the positive ion. Figure 2-12 is a depiction of charge transfer that can occur within an ionization chamber:

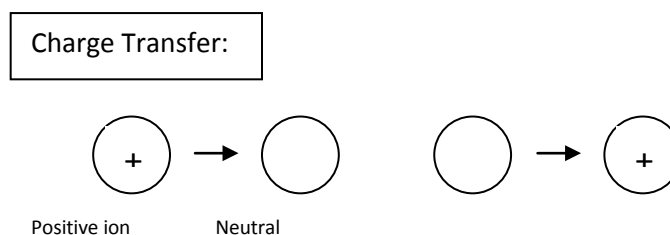


Figure 2-12: Charge Transfer (Adapted from Knoll 2000)

Electron attachment is a process when the free electron member of the original ion pair undergoes a collision with a neutral molecule within the gas and forms a negative ion (Knoll 2000). The negative ion that is formed has the same properties with the original positive ion formed in the ionization process, but with opposite electrical

charge. Figure 2-13 is a depiction of electron attachment which can occur within an ionization chamber:

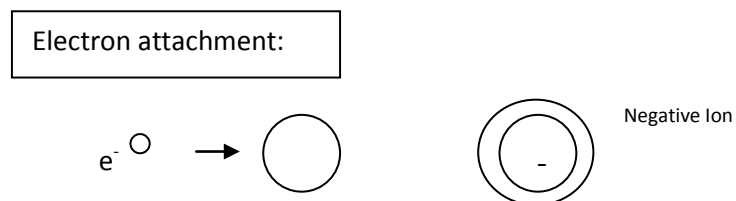


Figure 2-13: Electron Attachment (Adapted from Knoll 2000)

Recombination results from the collision between positive ions and free electrons in which the electron is captured by the positive ion and returns it to a state of charge neutrality (Knoll 2000). Conversely, the positive ion can undergo a collision with a negative ion in which the extra electron is transferred to the positive ion and both ions are neutralized. In both cases, the charge in the original pair is lost and will not contribute to the signal in the ionization chamber and the collection of ionization charge is lost. Figure 2-14 is a depiction of electron attachment which can occur within an ionization chamber:

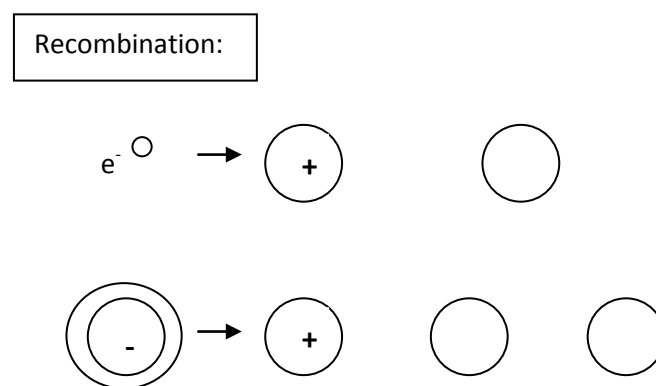


Figure 2-14: Recombination (Adapted from Knoll 2000)

An external electric field is applied to the ionization chamber and the ions and electrons in the gas will tend to move by electrostatic forces away from their point of origin (Knoll 2000). The net motion is a random thermal velocity with a net drift velocity and these two forces together make the movement of ions in a given direction. Positive ions have a drift velocity in the direction of the conventional electric field, while free electrons and negative ions drift in the opposite direction. The electric current within an ionization chamber is represented by the drift of positive and negative charges by the electrons and ions in the gas. When a given volume of gas is undergoing steady state irradiation, the rate at which the ion pairs are forming is constant. Figure 2-15 depicts the electrostatic forces within an ionization chamber.

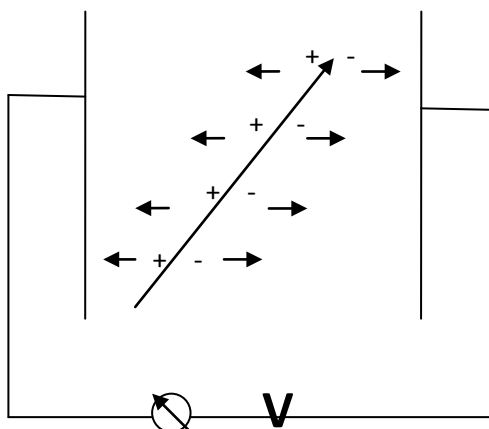


Figure 2-15: Ionization Current (Adapted from Knoll 2000)

In principle, the rate of ion formation will be exactly balanced by the rate at which ion pairs are lost from the detector volume, either through recombination or by diffusion or migration from the volume (Knoll 2000). If recombination is negligible and all the charges are collected, the steady state current produced is an accurate measure of the rate at which ions pairs are formed within the ionization chamber volume.

The design of a general ionization chamber consists of a volume of gas that is enclosed within a region with an applied electric field that can be created through an

external voltage. With no radiation penetrating the ionization chamber (equilibrium), the current flowing in the external circuit will be equal to the ionization current collected at the electrodes, and a sensitive ammeter placed in the external circuit can measure the ionization current (Knoll 2000). In the absence of an applied voltage, no net current should flow because no electric field will exist within the chamber's gas. The ions and electrons that are created within the chamber when no electric field is applied disappear either by recombination or by diffusion from the active volume. When the applied voltage is increased, the resulting electric field begins to separate ion pairs more rapidly and recombination is slowly diminished within the ionization chamber. As the voltage applied increases, the positive and negative charges are also swept toward the respective electrodes with increasing drift velocity, which reduces the equilibrium concentration of the ions within the gas and therefore further restraining recombination between the original creation of the ion pair and the collecting electrodes (Knoll 2000). The measured current in the ionization chamber is therefore dependent on the increasing applied voltage as these effects reduce the amount of the original charge that is lost. When the applied voltage is sufficiently high, the electric field is large enough to effectively suppress recombination to a negligible level, and all the original charges created through the ionization process contribute to the ion current (Knoll 2000). If the applied voltage is further increased, the current does not change because all charges are already collected and their rate of formation is constant. This region within the ionization chamber is called ion saturation, which most ionization chambers are conventionally operated (Knoll 2000).

When the voltage is significantly high to suppress recombination and other reactions, the current measured in the external circuit is an accurate indication of the rate of formation of all ion pairs created within the active volume of the chamber. Ion saturation can be detracted within an ionization chamber through several factors which make the chamber not at full operating potential. Recombination is the most important interaction within the ion chamber volume which is diminished through

ensuring that a large value of the electric field exists everywhere in the ion chamber volume (Knoll 2000).

Air is the most common fill gas and is one in which negative ions are readily formed. Air is required in ionization chambers designed for the measurement of gamma ray and x-ray exposure. The fill gas within the chamber is often at a pressure of one atmosphere, although higher pressures are sometimes used to increase the sensitivity.

Most ionization chambers are operated at extremely small currents, on the order of 10^{-12} A or less. For this reason, the leakage current through the chamber must be kept very small. Insulators are used between the electrodes to reduce the leakage because any leakage through these insulators will add to the measured ionization current and cause an unwanted component of the signal. Figure 2-16 depicts the insulators and guard rings composed inside the ionization chamber.

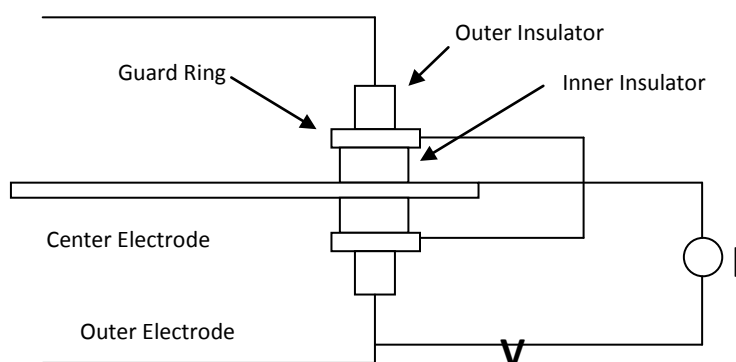


Figure 2-16: Insulators and Guard Rings (Adapted from Knoll 2000)

To aid the insulator in reducing leakage, a guard ring is also employed to reduce the effects of insulator leakage between the electrodes within the ionization chamber. The insulator separates the two electrodes, one insulator separating the conducting guard ring from the negative electrode and the other insulator separating it from the positive electrode (Knoll 2000).

The ionization current under typical conditions is much too small to be measured using standard galvanometer techniques. Thus, some type of amplification must be carried out so the current can be indirectly measured. For this application, an electrometer indirectly measures the current by sensing the voltage drop across a series resistance placed in the measuring circuit (Knoll 2000). Figure 2-17 depicts the measuring circuit of an ionization chamber and the electrometer used to measure the voltage drop.

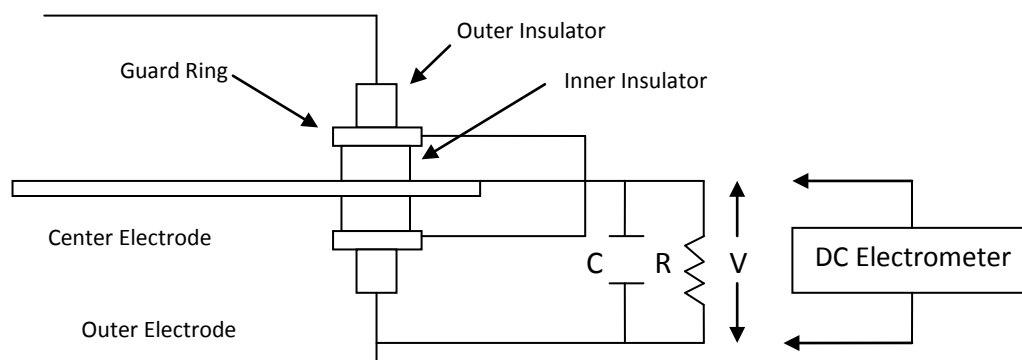


Figure 2-17: Measuring Circuit and Electrometer (Adapted from Knoll 2000)

Figure 2-18 depicts the electrometer used in the experiment.

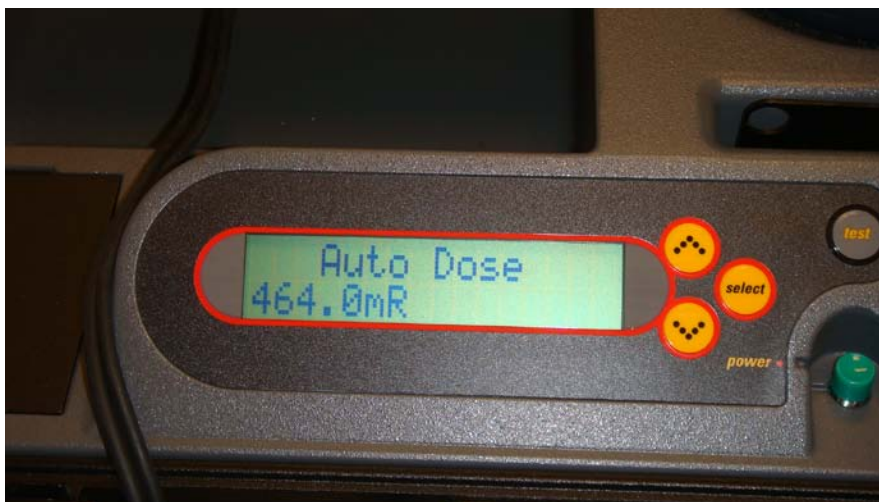


Figure 2-18: Electrometer

The voltage that is across the resistor, typically with a value of 10^9 - 10^{12} ohms, can be amplified and serves as the basis for the measured signal. Electrometer circuits must be dc coupled because any small drift or gradual change in component values therefore results in a change in the measured output current. A dc coupler is a device for interconnecting two circuits. This type of circuit must be frequently balanced by shorting the input and resetting the scale to zero so there is no drift in the current as you are operating the ionization chamber.

The radiation dose measurement within an air-filled ionization chamber is particularly well suited because exposure is defined in terms of the amount of ionization charge created in air. The fundamental SI unit (coulomb/kg) of exposure corresponds to the amount of x-ray radiation whose associated secondary electrons create an ionization charge of 1 coulomb per kilogram of dry air at STP (Knoll 2000). The ionization chamber, under the proper conditions for operation, can determine the ionization charge in an air filled chamber and can give an accurate measure of the exposure, and a measurement of the ionization current will indicate the exposure rate. The measurement of exposure from an ionization chamber uses the principle of

compensation because secondary electrons that are created have a very long range in air. Since electrons have a long range in air, it would be impractical to build an instrument that large to carry out such a measurement directly. The compensation principle takes into account that if the test volume of air within the ionization chamber is surrounded by an infinite sea of equivalent air that is also subject to the same exposure over the course of the measurement, an exact compensation will occur (Knoll 2000). The surface dose of the ion chamber is where compensation within the ion chamber volume will have an affect. Figure 2-19 depicts the principle of compensation in air and the x-ray exposure on the surface of the phantom when backscatter is considered.

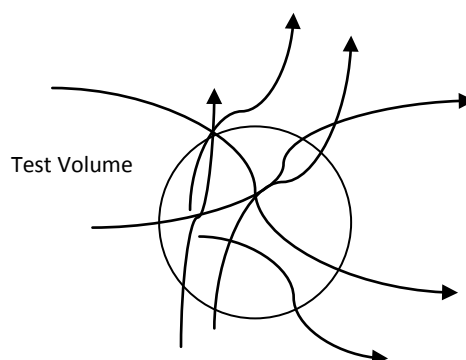


Figure 2-19: Compensation (Adapted from Knoll 2000)

Thus, the ionization charge that is created outside the test volume from secondary electrons formed in the surrounding air is exactly balanced by charge created within the test volume from secondary electrons (Knoll 2000).

For an air-filled ionization chamber, the exposure rate in C/kg*s is given by the ratio of the saturated ion current I_s (in amperes) to the mass M (in kg) contained in the chambers active volume (Knoll 2000). The air mass M is calculated from a measurement of the chamber volume and the density in STP. As mentioned above, because the signal is very low, sensitive electrometers along with an ideal chamber

design are required to minimize the leakage current within the chamber. The ion current I_s within the chamber is proportional to the mass of the gas. The ion current can be increased by two ways, either increasing the chamber volume or the pressure of the gas.

The ionization chamber can be applied to the indirect measurement of absorbed dose, the energy absorbed per unit mass. The Bragg-Gray principle is the technique which the absorbed dose measurement is based off of and can be deduced by the ionization produced in a small gas filled cavity within a material (Knoll 2000). If a cavity ionization chamber is built with wall material whose radiation absorption property is similar to that of tissue, then according to the Bragg-Gray principle, the amount of ionization produced in a small gas-filled cavity surrounded by a solid absorbing medium is proportional to the energy absorbed by the solid (Cember 2009). The formula is $D_M = W S_M P$, where W is the average energy loss per ion pair formed in the gas, S_M is the relative mass stopping power of the material to that of the gas, and P is the number of ion pairs per unit mass formed in the gas. The ionization chamber cavity should be small compared to the range of the primary or secondary charged particles associated with the radiation so that its presence does not greatly affect the particle flux (Knoll 2000). The solid medium should be large compared with the range of the secondary electrons so that electronic equilibrium is established at the inner walls of the cavity. The ionization chamber consists of both a solid medium, which is the wall material surrounding the chamber, and a cavity which is its internal gas filled volume. The absorbed dose in biological systems is of great interest in radiation protection, so a tissue-equivalent ion chamber is applied in which the wall material is made of material with similar composition to that of tissue (Knoll 2000).

The ionization chamber used in the experiment is a RadCal 9095 operated in the auto-dose function. The ionization chamber has an accuracy of plus or minus 4 percent and a correction factor of 1.22.

Figure 2-20 is a depiction of the RadCal 9095 Ionization chamber used in the research.



Figure 2-20: Ionization Chamber

2.9 VARSKIN

The VARSKIN code is a tool for assessing doses from skin contamination, including hot particles (Varskin 2006). The original VARSKIN code was developed for use by the NRC staff to calculate skin dose for regulatory requirements. Both the industry and academia have been interested in using the code for various research and development projects. The Center for Nuclear Waste Regulatory Analyses division of the NRC re-developed the code to calculate skin dose from radioactive skin contamination, and has recently revealed a new type of radioactive skin contamination. This new type of skin contamination is called “hot” particles and differs from uniform skin contamination because the particles have a thickness associated with them and previous VARSKIN codes don’t account for self absorption. Moreover, these hot particles mainly result from radioactive spills that are outside of protective clothing which result in a cover thickness which must be added to the parameters.

The dose from VARSKIN is computed at any depth in skin or in a volume of skin from point, disk, cylindrical, spherical, and slab sources. Since this research is only interested in the photon dose, and not the beta dose, the source parameter will be a point source. Although VARSKIN is essentially for hot particles, the program will be designed to simulate some of the parameters of an x-ray machine. The major drawback will be that the VARSKIN model only accounts for an air gap of 5 cm, which the x-ray machine has a source to image distance (air gap) of forty inches. Furthermore, VARSKIN doesn't take into account an x-ray intensity spectrum which is produced by an x-ray machine. An average photon energy will be used instead of a spectrum which could also deviate the dose. Another parameter which is hard to model is the number or intensity of x-ray photons within the x-ray beam. Since each machine has a different energy conversion to bremsstrahlung, it is hard to determine the exact number of x-ray photons for a specific x-ray machine.

3.0 TLD Experimental

3.0.1 TLD Annealing

The TLD has three distinct heating regions in which supply the proper readout that is correlated to the exposure. The three regions include pre-irradiation anneal, post-irradiation anneal, and read. The pre-irradiation anneal effectively zeros the TLD chips and is done before the chip is used for exposure. The TLD readout process involves an annealing procedure prior to exposure of the TLD's as to completely zero the TLD chips. The pre-irradiation anneal consists of baking the chips at 400 degrees Celsius for one hour. The TLD's are ready to be exposed to a radiation source after the pre-anneal procedure. The post-irradiation anneal is used to eliminate any lightly trapped electrons within the band and is often called the low-temperature dosimetry traps. These lightly trapped electrons are quick to release because of the very small amount of excess energy required to liberate them. The post-irradiation anneal requires a temperature at 100 degrees Celsius for ten minutes. The TLD chips are ready to be readout in the TLD reader after they have cooled down from the post-

irradiation anneals. If the post-irradiation anneal is not done after the exposure, then the lightly trapped electrons will be included in the readout and may overestimate the dose signal from the TLD chip. The read region of the TLD chip correlates to an approximate temperature of 195 degrees Celsius and is the temperature region where most of the exposure is read out. Figure 3-1 depicts the TLD heating regions relative to a glow curve output.

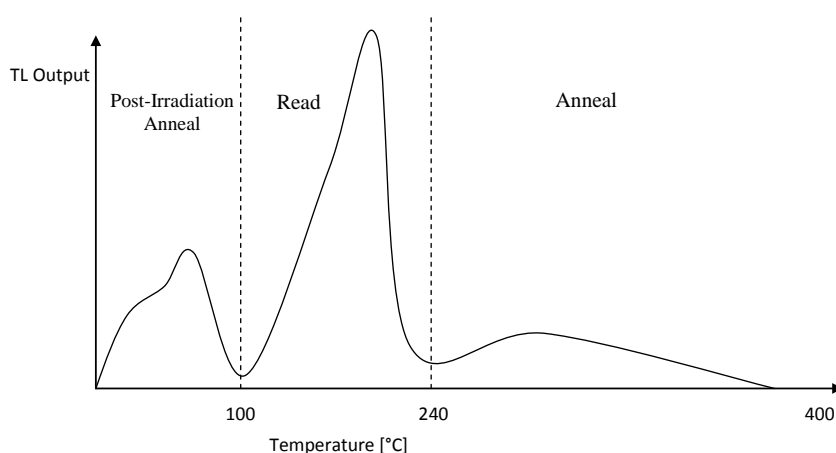


Figure 3-1: TLD Glow Curve

3.0.2 Processing TLD's

The TLD reader must be purged with nitrogen gas for 30 minutes to remove possible charge accumulation inside the reader chamber, which must be done before processing the TLD chips. After the purging procedure, 10 dark and 10 light current readings are taken before the exposed TLD's are processed. This is done to ensure that the system is stable and the reader is within the range of dark and light current readings. The dark current readings should be within the range of 590-610 nano-Coulombs. After taking five or six dark current readings, the TLD reader should be fairly stable and the readings will not have much variation. Once the TLD reader is stable and the dark current readings have stabilized, light current readings will be taken to make sure that the system has been established.

The TLD chips are read by placing a TLD chip on the planchet and closing the TLD tray door. After the door is shut, approximately 30 seconds should be given to the TLD reader so the system can purge before pressing the read button. Once the read button is pressed, the planchet is initiated to start the heating process. The TLD reader is programmed to record the total photon emissions from the TLD chip with a planchet temperature between 100 °C and 240 °C. The TLD-100's have a readout temperature at 195 °C which places the planchet temperature in an appropriate range. The total amount of photon emissions will be read out in a digital display in the unit of nano-Coulombs. Once the TLD chips are processed, another 10 dark and 10 light current readings are taken to make sure the system is still stabilized during the readout process.

3.0.3 Calibration Curves

The calibration curve is the key component to reading out the correct dose on a specific TLD. The calibration curve is the delivered dose (mrem) to the TLD versus the light output (nano-Coulombs). The calibration curve determines if the TLD reader is consistent with the output (nC) and the delivered dose (mrem) to the TLD's. The TLD reader will slowly heat the TLD and the amount of photons released from the TLD will be measured by the photomultiplier tube. The number of photons is recorded in nano-coulombs and will be correlated with the delivered dose. The calibration curve will supply the unknown dose to the experimental TLD's using the light photons released from the chip and read by the photomultiplier tube. The calibration TLD's were exposed to a 10 mCi Pin wheel Radium-226 source for varying amounts of time to deliver a known dose to the TLD. A total of five TLD's were used for each delivered dose interval to account for statistical variation within the TLD chips. Once the TLD's were exposed, a post-irradiation anneal was done, and then the TLD's are read-out in the TLD reader.

Table 3-1 shows the desired dose versus the exposure time.

Desired Dose (mrem)	Exposure Time (sec)
10	382
15	573
20	765
25	956
30	1147
40	1530
50	1913
60	2295
70	2677
75	2869
100	3826
125	4782
140	5354
150	5738
160	6118
175	6695
200	7651
225	8607
250	9564
275	10520
300	11477
325	12433
350	13389
375	14346
400	15302
425	16258
450	17215
475	18171
500	19127

Table 3-1: Exposure Time for TLD Calibration

Figure 3-2 shows the low dose calibration curve with standard deviations and figure 3-3 displays the high dose calibration curve with standard deviations.

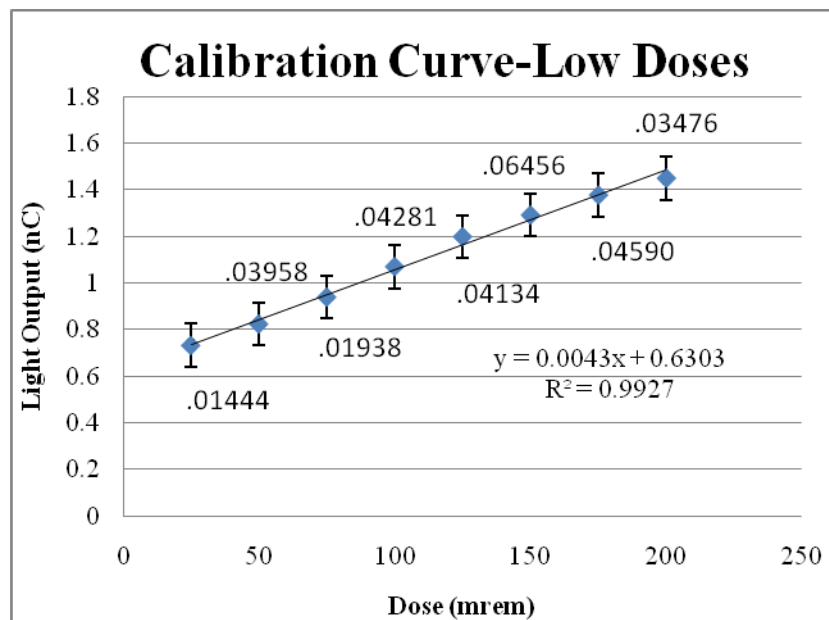


Figure 3-2: Low Dose Calibration Curve

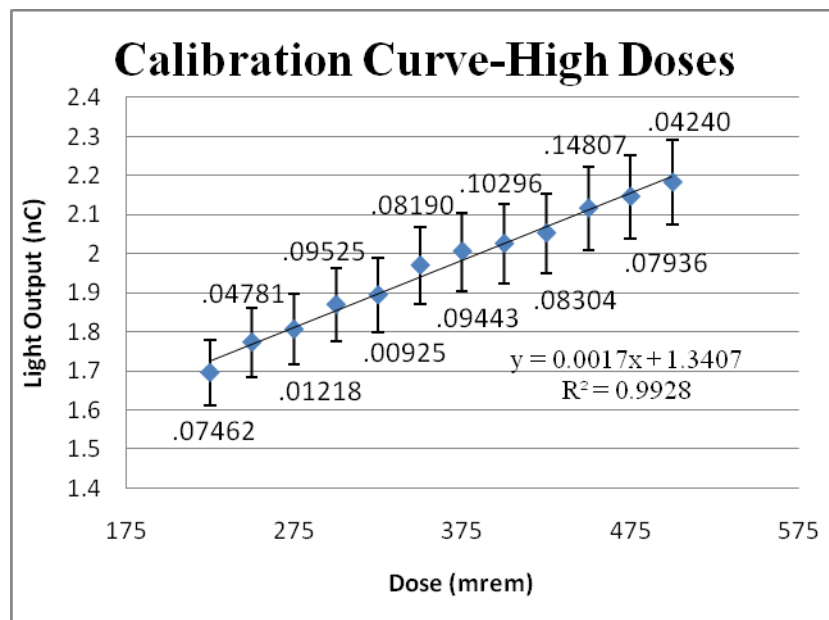


Figure 3-3: High Dose Calibration Curve

The calibration curves for both low and high doses are significantly linear. This results in the calibration curve being relevant and demonstrates that the system is working properly. The calibration curve will be paramount in determining the dose from the experimental TLDs.

4.0 Factors Affecting Dose

The dose from an x-ray machine with increasing depth into skin and tissue will depend on many factors. Of these factors: beam energy (tube voltage), tube current, depth, type of x-ray procedure, field size, distance from source, backscatter, the type of electron interaction, filtration and beam collimation are the major factors that affect the dose as depth increases in skin and tissue. The type of x-ray procedure is an AP abdomen. The beam energy used in this research is 80 keV which is the normal energy used for an abdominal x-ray procedure. The tube current was set at 160 mA, which is also standard for this type of procedure. The field size is an 8 x 8 inch Plexiglas water equivalent phantom and was collimated to a 20 x 20 cm field which is directly within the field size. The distance from the source is 40 inches which is the recommended distance for an x-ray procedure. Backscatter from the Plexiglas may be relevant within this research and will be considered as both the TLD's and the ion chamber dose are compared.

When accelerated electrons produced in the x-ray tube interact with the target material, there are four typical electron interactions that may occur. These four interactions include electron scattering, electron capture, characteristic x-ray production, and bremsstrahlung production of which three of these interactions produce x-rays. Typically, only one percent of the energy from the electrons striking the target is transferred to bremsstrahlung production (the major source of x-ray production). To determine radiation exposure, the number or intensity of x-rays produced from the target must be determined. Assuming that the target is thin, and that each electron from the x-ray tube only goes through one interaction with the target, a spectrum of x-ray intensities will be produced. Although for the VARSKIN

application, an average photon energy must be used since there is no way of determining the correct spectrum of energies coming from the specific x-ray machine used. Since the typical target is thick, the electrons are more likely to interact more than once in the target which will greatly reduce the energy of the bremsstrahlung photons produced and the spectrum of intensities will decrease.

Another factor that is going to affect the dose from the x-ray machine is added filtration. Most x-ray machines have beam filtration from the x-ray tube housing or added filtration that the beam must pass through. Taking these beam filtration factors into considering, there is a kV specific curve of photon intensities that can be generated that start at zero intensity for some maximum kVp value, rises to a maximum, and finally drops off due to the attenuation of the filtering material. Although these output curves vary from one x-ray tube to the next due to variations in any of the parameters specified.

X-ray production will also vary over time due to wear on the anode or target. As the anode is bombarded by electrons over time, the target will become pitted and can eventually crack and will result in less x-ray production. Given that x-ray production will vary over time, it would be very difficult to calculate the actual output for the same x-ray tube without knowing the exact conversion efficiency of input electrons to output x-rays at any given time.

The intensity of the x-ray beam is related to the following parameters: (1) Intensity is directly proportional to the atomic number (Z) of the target, (2) Intensity is directly proportional to current (mA), (3) Intensity is directly proportional to the voltage, and (4) Beam quality or hardness will increase with added filtration in the beam.

5.0 Experimental

5.1 Phantom Design

The material used for tissue and skin equivalence is Plexiglas and is used in the field for both calibration and experimental procedures with x-ray machines. The phantom that was used is composed of an 8 x 8 inch slab of Plexiglas which will simulate the patient as dose enters the skin and travels through the tissue at different increments. Figure 5-1 depicts the phantom design used in the experiment.

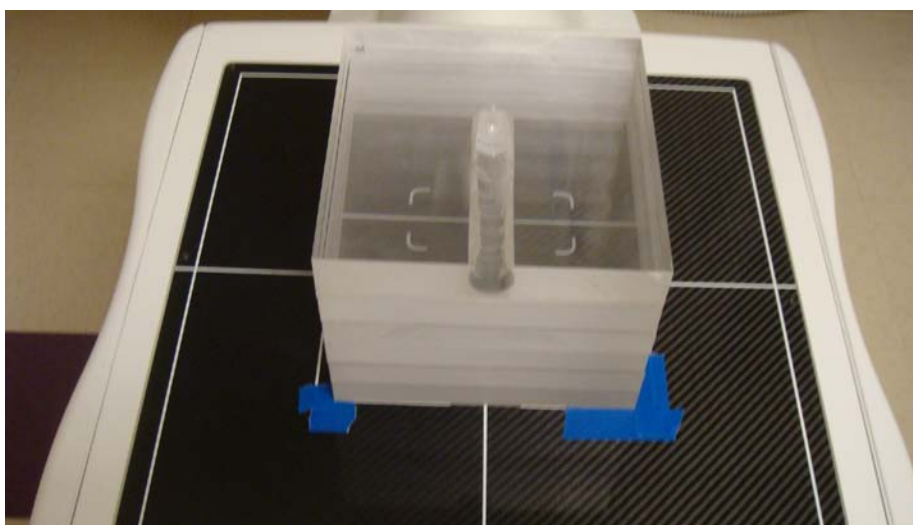


Figure 5-1: Phantom Design

It is recommended that the phantom designed for measurements on all field sizes should have an area approximately 30 cm x 30 cm and a thickness of 20 cm (which approximates to a trunk anteroposterior view) (Martin 1998). The phantom that is designed will consider backscatter and the average thickness of a trunk of a human. By placing the phantom in the center of the collimators, the ion chamber and TLD will be measured for skin and tissue dose measurements with increasing depth. The phantom Plexiglas material will simulate the patient during an abdominal x-ray procedure which will account for a homogenous material. The phantom thickness is 6.5 inches thick and will be used to approximate the size of an average human abdomen. The x-ray machine will be collimated to produce a 20 x 20 cm field size

area to simulate an abdominal x-ray procedure. The collimation and phantom are designed to reproduce the anatomy of a human abdomen so the experiment can measure skin and tissue dose as accurately as possible.

5.2 Experimental Procedures

Skin dose and tissue dose will be measured at different depth increments with both an ion chamber and TLD's. The doses from the ion chamber and TLD's will be compared at the different depth increments to experimentally determine the dose response of each detector as the dose decreases with skin and tissue depth. The percent difference will be calculated to measure how close the two detectors dose response for each depth is.

Skin depth increments will be much smaller than tissue depths because the skin is much thinner than tissue. The human body has an average of about 5-6 mm of skin containing both the epidermis and dermis layers of the skin (Martini 2006). Thus, skin depth increments will be in the millimeter range representing: 1/16 inch (1.5875 mm), 3/32 inch (2.38125 mm), 1/8 inch (3.175 mm), 3/16 inch (4.7625 mm), and 1/4 inch (6.35 mm) depths. The dose will be measured at each increment with both an ion chamber and TLD's.

The tissue dose depth increments will be larger considering there is a thicker layer of tissue underneath the epidermis and dermis layer of the skin. The tissue dose depth increments will be 1/4 inch (6.35 mm)(0.635 cm) and the dose will be measured with both an ion chamber and TLDs up to 2 inches. Since the thickness of the phantom is 6.5 inches, the tissue dose depth increments will go in 1/4 inch depths until a thickness of 2 inches is reached. After 2 inches, 1 inch increments will go to the bottom of the phantom where this will correspond to the exit dose at the bottom of the phantom. Quarter inch depths were not measured throughout the entire phantom due to time constraints with the x-ray machine and the number of TLDs needed to accomplish each 1/4 inch depth through the 6.5 inch phantom.

The measurements will correspond to dose at different depths within the human body but using only a homogenous tissue equivalent material. Thus, we can assume that there is only one type of tissue being irradiated in the phantom which has a tissue equivalence of water. We can also assume that there is a layer of fat tissue underneath the skin, so that the type of tissue being irradiated within the body is adipose tissue.

Since the skin is very thin, the type of TLD used for skin dose must be thin as well. By using a thinner TLD, we can assume that the thickness of the TLD is negligible. The TLD-100's have a dimension of 0.3175 cm x 0.3175 cm with a thickness of 0.0152 cm (150 microns) and will be used for skin and tissue dose. The thin TLD will be useful for skin dose measurements because the thickness of the TLD will not have to be accounted for and dose measurements will be as thin as possible for skin dose since these TLD's are the thinnest manufactured.

The x-ray tube should be positioned where the tube height, focus to table distance, should be set to that used in clinical practice (Martin 1998). This standard distance is 100 cm (39.37 inches). The top of the x-ray table should be 100 cm from the x-ray tube, also known as the source to image distance. The phantom will be placed on the x-ray table and the detector (either an ion chamber or TLD) will be placed on the top of the phantom and this distance from the table is the object to detector distance. The distance between the top of the phantom and the x-ray tube is called the source to object distance. This type of set-up is called an overcouch x-ray tube and will be the design used in this experiment (Martin 1998).

Figure 5-2 displays the x-ray machine tube height positioned for the experiment.



Figure 5-2: X-ray Machine

The collimation will be set just within the field size of the phantom which is 20 x 20 centimeters. Since the source to image distance is 40 inches, the collimators will likely be fully opened to satisfy the field size of the phantom. The 20 x 20 cm collimation within the tube is set to an almost fully open collimation system. The downside to having a large field size is backscatter. Backscatter occurs when an x-ray photon transfers its energy to an electron which interacts in the Plexiglas and is sent back in the opposite direction. Backscatter from the patient increases with increasing field size and may play a large role in the dose at different depth increments (Balter 2010). It has been documented that the backscatter factor is in the range of 25%-40% (Balter 2010). Skin dose is higher than air KERMA at the skin by a field size independent factor of 1.06 (Balter 2010).

The ion chamber and TLD surface dose measurements will be measured on the surface of the 6.5 inch phantom. The surface dose on the skin will be measured by placing the TLD directly on the phantom with no Plexiglas separating the x-ray beam and the surface of the TLD. The surface dose for the ion chamber will be measured by inserting the ion chamber into a 1-1/4 inch sheet of Plexiglas that has a 1 inch hole

drilled directly on the surface of the Plexiglas to just fit the ion chamber diameter. The 1 inch hole that is drilled across the surface of the Plexiglas will expose the ion chamber on one side so that a surface dose can be measured. Sheets of Plexiglas with various thicknesses will be placed over the two detectors to measure the skin and tissue dose as the depth increment changes for the TLD and the ion chamber. The Plexiglas will sit on top of the TLD's without any air gaps between the Plexiglas surfaces. Figure 5-3 displays the surface dose for the ionization chamber.

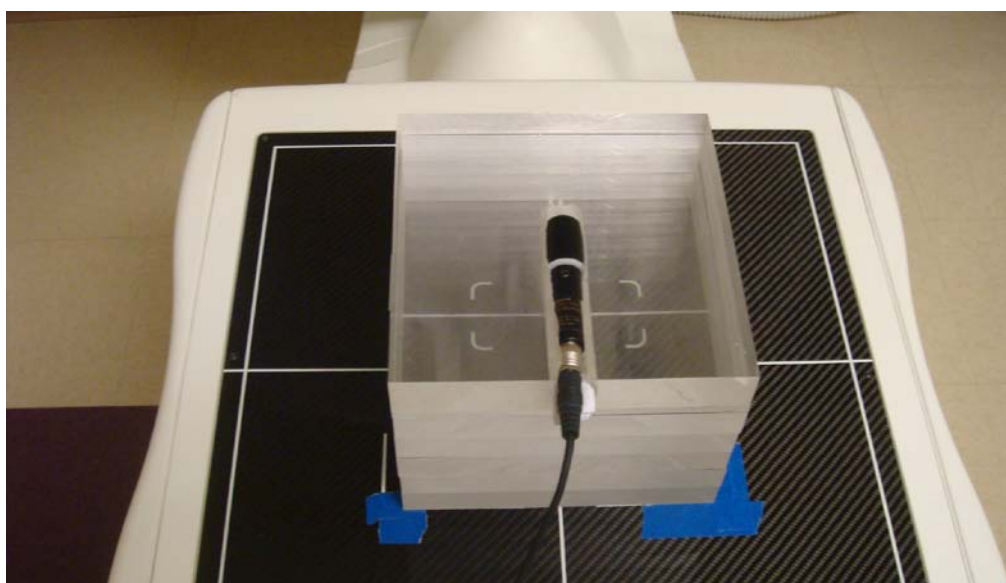


Figure 5-3: Surface Dose for Ion Chamber

To measure the first skin depth increment, a 1/16 inch (1.5875 mm) slab of Plexiglas will be placed over the top surface of the ion chamber and the TLD's so that only the 1/16 inch of Plexiglas covers the detector. To measure skin dose with increasing depth, sheets of Plexiglas will be stacked on the top of the ion chamber and TLD's with the phantom underneath until a dose measurement of a ¼ inch (6.35 mm) of skin is measured.

The tissue dose measurements will start at a ¼ inch, since that is the approximate thickness of the outer skin which is covering the tissue. The ion chamber will be inserted into a Plexiglas sheet with a ¼ inch of Plexiglas placed on the top surface of

the ion chamber. The TLD's will be placed on top of the phantom with a $\frac{1}{4}$ inch of Plexiglas covering the TLD's. As the depth increments increase from a $\frac{1}{4}$ inch, the depth will be increasing within the phantom (into the tissue of a human). The dose depth will start at a $\frac{1}{4}$ inch and increase an additional $\frac{1}{4}$ inch each different increment up to 2 inches and then 1 inch increments will be used until the tissue dose is at the bottom of the phantom (6.5 inches). Figure 5-4 depicts the exit dose for the ionization chamber.

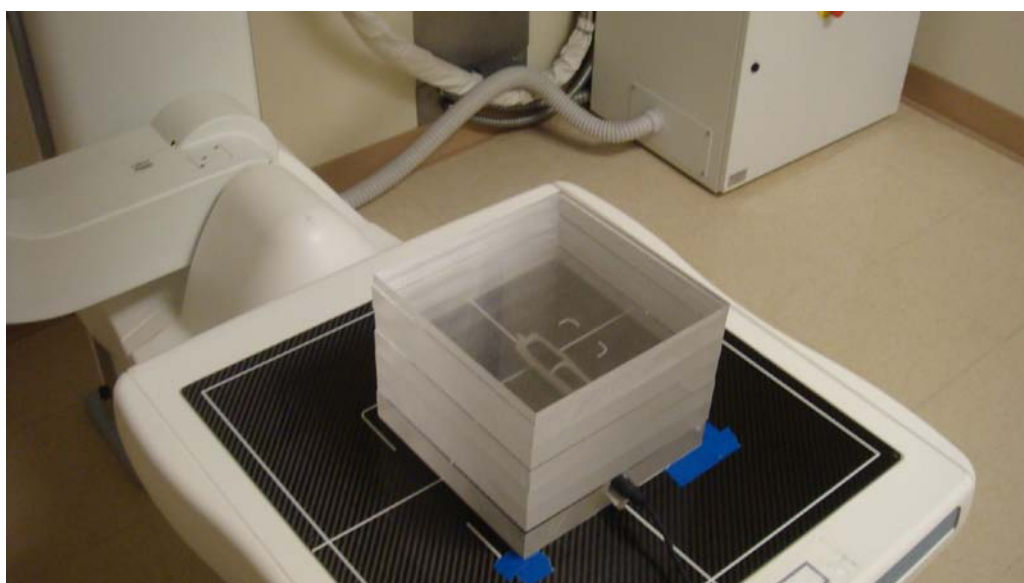


Figure 5-4: Exit Dose for Ion Chamber

6.0 Calculations

The dose to each set of TLD's at a certain depth was found by taking the mean TLD readout (nano-coloumbs) and linearly interpolating the dose from the calibration curve.

Figure 6-1 depicts the linear interpolation equation and the representation of the data points.

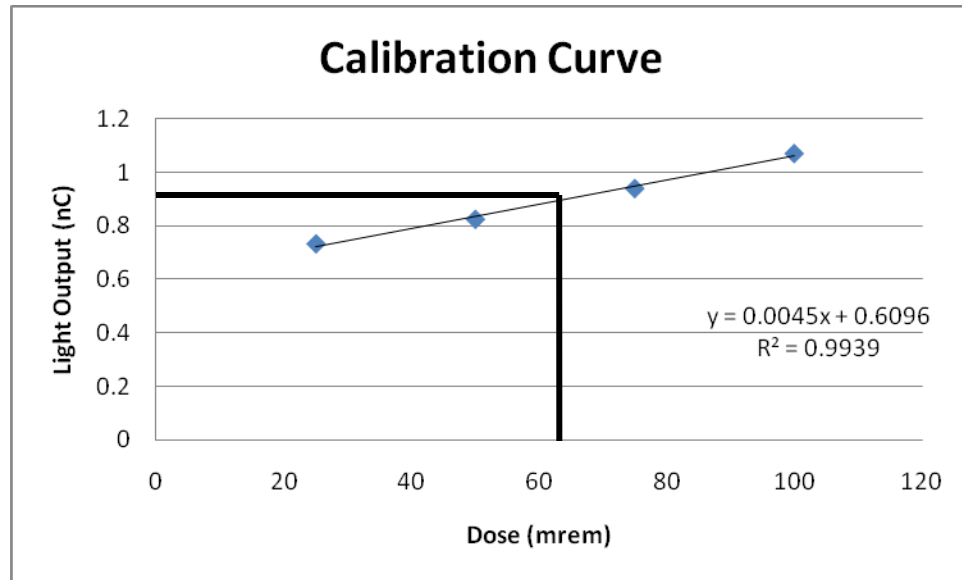


Figure 6-1: Linear Interpolation Graph

6.1 VARSKIN Calculations

For the VARSKIN model, the parameters of the x-ray machine must be accounted for so we can determine if the dose at each depth is comparable. To figure out the number of bremsstrahlung x-rays coming from the x-ray beam, a factor of one percent was used which accounts for the total amount of energy that is converted to bremsstrahlung production. To determine the number of electrons striking the tungsten target with a current of 160 milli-amperes for a quarter of a second, this is the calculation that was done:

$$1 \text{ mA} \cdot \text{s} = (10^{-3} \text{ coulomb/sec})(\text{sec}) / (1.6 \cdot 10^{-19} \text{ coulomb/electron}) = 6.25 \cdot 10^{15} \text{ electrons}$$

$$\text{Total \# of electrons} = (160 \text{ mA}) \cdot (.25 \text{ sec}) \cdot (6.25 \cdot 10^{15} \text{ electrons/mA} \cdot \text{sec}) = 2.5 \cdot 10^{17} \text{ electrons}$$

The total amount of energy that is converted from this number of electrons is one percent. The energy value that was used is 80 keV, and 1 percent of 80 is .8 keV converted to bremsstrahlung photons. Here is the calculation:

$$80 \text{ keV} * .01 = .8 \text{ keV}$$

$$(2.5 * 10^{17} \text{ electrons}) * (.8 \text{ keV}) = (2.0 * 10^{17}) * (.01) = 2.0 * 10^{15} \text{ photons}$$

Since an x-ray machine has a wide spectrum of x-ray energies emitted from the tungsten target, an average energy was used to determine the number and intensity of the bremsstrahlung photons. The energy that was used is 80 keV, and the average energy is 32 keV.

$$\text{Total \# of Photons} = (2.0 * 10^{15}) / 32 \text{ keV} = 6.25 * 10^{13} \text{ photons}$$

6.2 Hand Calculations

Since there are many factors that play a large role in the dose from an x-ray machine (as mentioned above), hand calculations for surface dose are not practical in this situation. Hand calculations to correlate the parameters of an x-ray machine are extremely hard to replicate because of the different parameters involved. Currently, there is no hand calculation that has been accepted in the health physics field for the surface dose of an x-ray machine.

The absorbed dose can be calculated by using the surface dose and the appropriate transmission factor. The transmission factor is calculated by taking the negative exponent of the material density times the mass attenuation coefficient times the depth (cm). The absorbed dose at a certain depth in skin or tissue is calculated by multiplication of the surface dose (mR) and the transmission factor. The following equation represents the absorbed dose:

$$\text{Absorbed Dose} = \text{Surface Dose} * \text{Transmission Factor} (e^{-(\mu/p)(p)(cm)})$$

7.0 Results

The TLD experimental dose results were found by using the mean TLD readout in nano-Coloumbs and linearly interpolating the dose from the calibration curve. The mean TLD experimental result for each depth was used to define a single result value. The standard deviation of the TLD's per data point was used to determine the error for the single reported value. Table 7-1 reports the TLD readout and the standard deviation for each single readout value.

Depth (cm)	TLD Readout (nC)	St. Dev. (σ)(nC)
0	2.1486	0.105578617
0.15	2.141	0.028242993
0.39	2.13425	0.048396797
0.47	2.11	0.12369519
0.63	2.052	0.046407973
1.27	2.0125	0.071940948
1.90	1.99	0.130909511
2.54	1.922	0.068888194
3.17	1.8646	0.191330081
3.81	1.809	0.0222441
4.44	1.7346	0.079882414
5.08	1.544	0.195322298
7.62	1.2164	0.018215378
10.16	0.951	0.010874282
12.70	0.8978	0.016754104
15.24	0.8178	0.008526429
16.51	0.7892	0.00491935

Table 7-1: TLD Readout

The ionization chamber also has a statistical variation within its readings. Three separate readings were taken at each depth. The mean ionization chamber experimental dose result for each depth was used to define a single result value. The standard deviation of the ionization chamber readings per point was used to determine the error for the single reported dose value.

Table 7-2 depicts the mean dose and the standard deviation for each ionization chamber dose.

Depth (cm)	Dose (mrem)	St. Dev.(σ) (mR)
0	457.36	2.11266
0.15	453.8	1.15326
0.39	445.3	1.30767
0.47	443	1.15326
0.63	431	0.34641
1.27	395.16	0.05774
1.90	359.46	0.40415
2.54	324.6	0.10000
3.17	292.7	0.20000
3.81	264.1	0.10000
4.44	236.96	0.11547
5.08	211.96	0.15275
7.62	134.4	0.10000
10.16	82.74	0.09018
12.70	74.58	0.04619
15.24	48.89	0.01732
16.51	37.61	0.03512

Table 7-2: Ionization Chamber Dose

The standard deviation for the surface dose is much larger than for the doses at the bottom of the phantom due to the spectrum of x-ray energies which can deviate from one x-ray exposure to the next. The x-rays at the surface of the phantom have a spectrum of energies which creates a large fluctuation in the dose at the surface. As you penetrate into the phantom, the low energy x-rays are taken out of the x-ray beam, which is called beam hardening. The absorbed dose near the bottom of the phantom is from higher energy x-rays and low energy x-rays are not included in the dose measurement.

The dose between the ionization chamber and the TLD can be considered “comparable” if they are within five percent of each other. The dose response between the ionization chamber and the TLD with skin and tissue depth was found to be equivalent. The dose response between the ionization chamber and the TLD at each depth are within five percent and can be considered comparable. Table 7-3 depicts the dose at each depth for both the ionization chamber and the TLD and the percent difference.

Depth (cm)	Ion Chamber (mrad)	TLD's (mrad)	Percent (%)
0	457.36	469.09	2.56%
0.15	453.80	464.77	2.42%
0.39	445.30	460.93	3.51%
0.47	443.00	447.57	1.03%
0.63	431.00	417.45	-3.14%
1.27	395.16	383.71	-2.90%
1.90	359.46	369.29	2.74%
2.54	324.60	338.76	4.36%
3.17	292.70	298.18	1.87%
3.81	264.10	276.26	4.60%
4.44	236.96	233.9	-1.28%
5.08	211.96	210.8	-0.52%
7.62	134.40	137.15	2.05%
10.16	82.74	81.54	-1.45%
12.70	74.58	73.38	-1.61%
15.24	48.89	48.12	-1.57%
16.51	37.61	39.18	4.17%

Table 7-3: Percent Difference Between Ion Chamber and TLD

Figure 7-1 displays the skin dose comparison of the ionization chamber and the TLD.

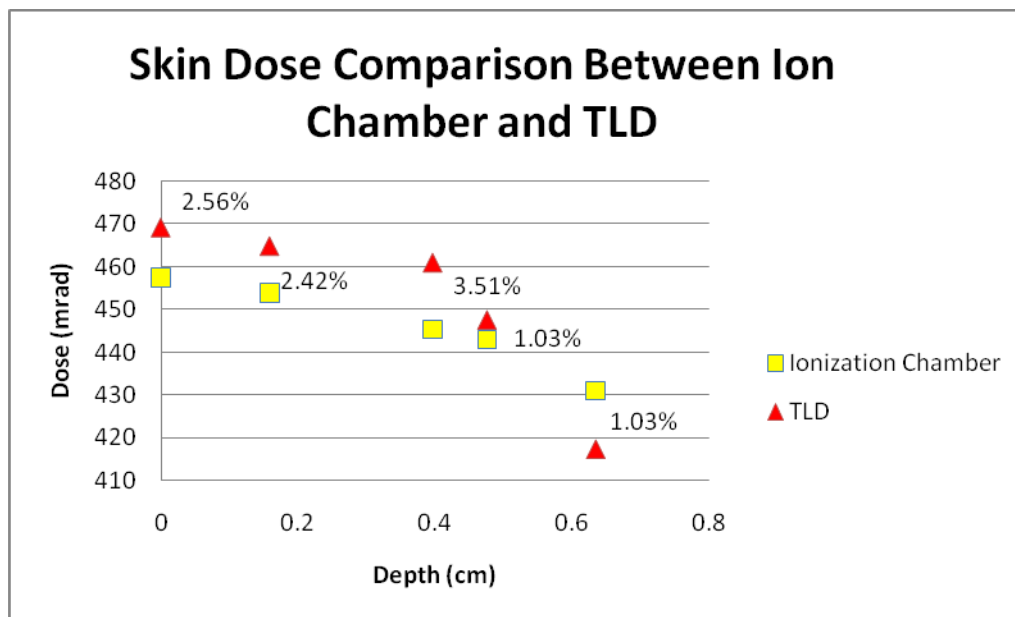


Figure 7-1: Skin Dose Comparison Between Ion Chamber and TLD

Figure 7-2 displays the tissue dose comparison of the ionization chamber and the TLD

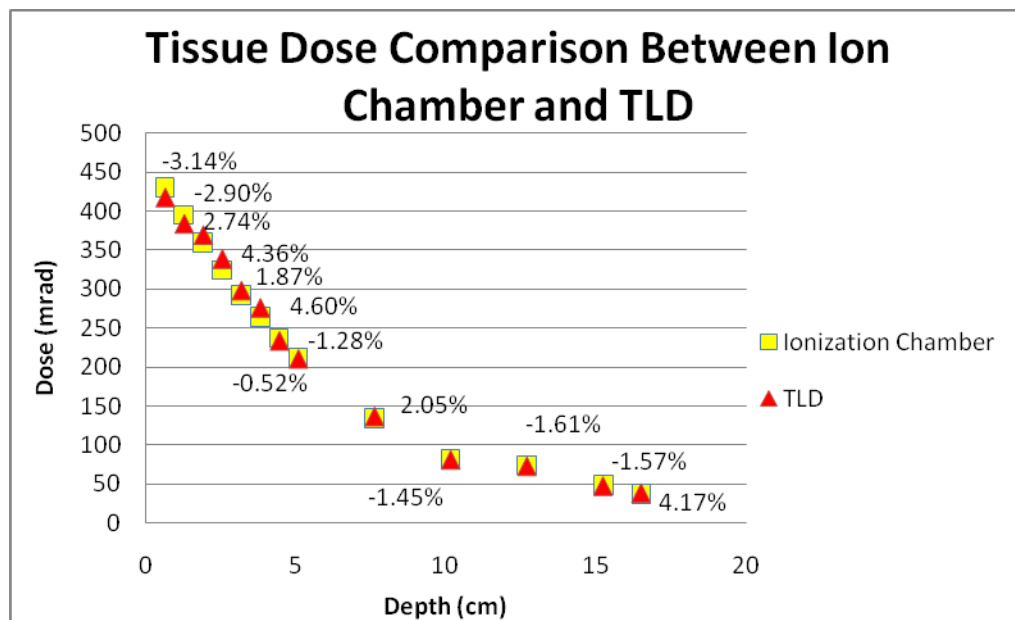


Figure 7-2: Tissue Dose Comparison Between Ion Chamber and TLD

Figure 7-3 displays both the skin and tissue dose comparison of the ionization chamber and the TLD.

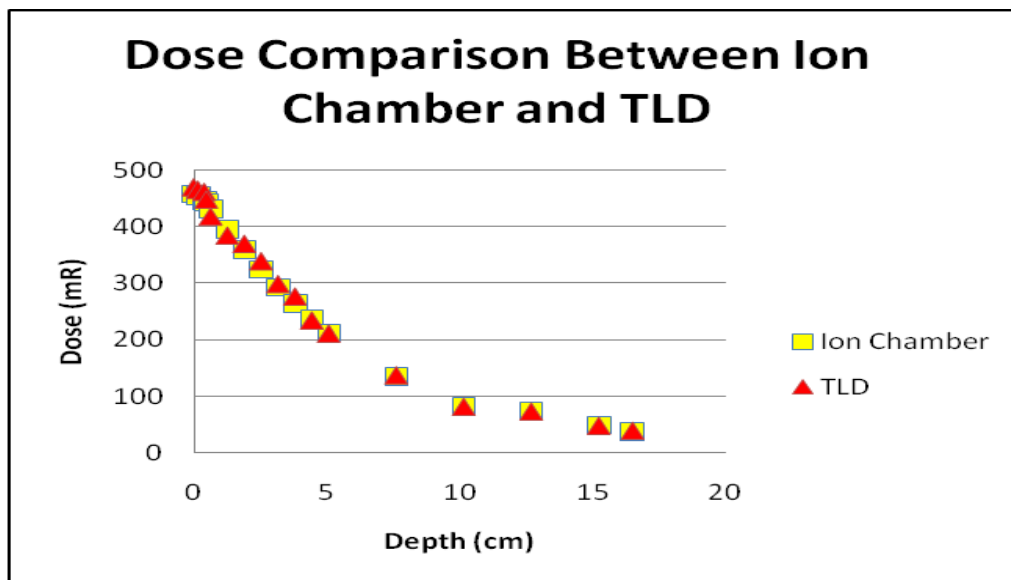


Figure 7-3: Dose Comparison Between Ion Chamber and TLD

The VARSKIN program was also compared to the ionization chamber and TLD with skin and tissue dose. The VARSKIN program was set up to match the experimental design of the x-ray machine as close as possible within its programmable limits. The VARSKIN program is not appropriate to compare with the x-ray machine because the program is used for skin contamination. The VARSKIN program was set to stipulate three skin averaging areas to consider the thickness of the TLD chip ($.01524 \text{ cm}^2$), the thickness of the ion chamber (2.5 cm^2) and to comply with the NRC skin averaging area of 10 cm^2 .

The dose comparison between the VARSKIN 4 program, Ionization chamber, and TLD for a skin averaging area of $.01524 \text{ cm}^2$ (TLD) is displayed in Figure 7-4.

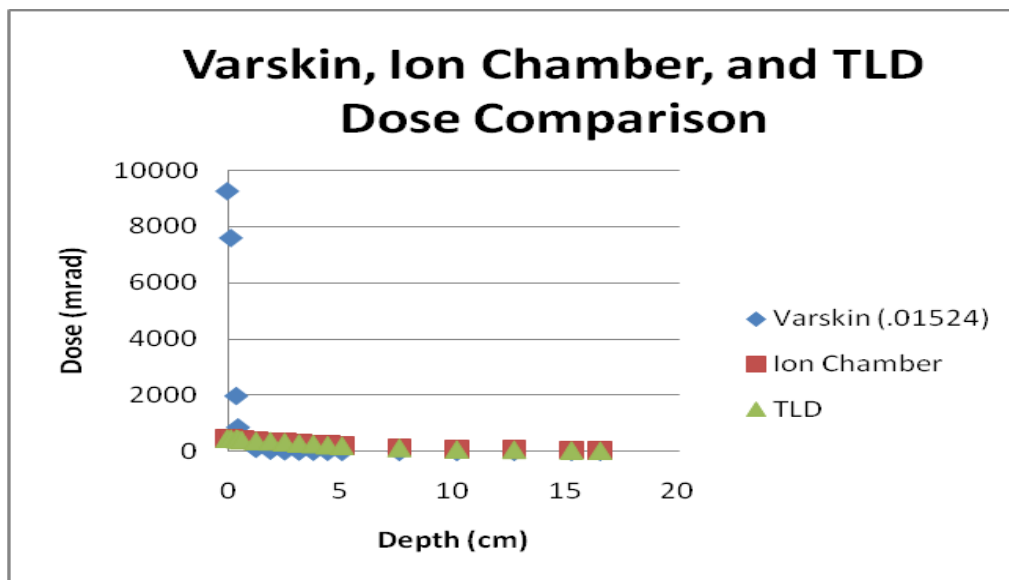


Figure 7-4: Varskin, Ion Chamber and TLD Dose Comparison ($.01524 \text{ cm}^2$)

The dose comparison between the VARSKIN 4 program, Ionization chamber, and TLD for a skin averaging area of 10 cm^2 (regulation) is displayed in Figure 7-5.

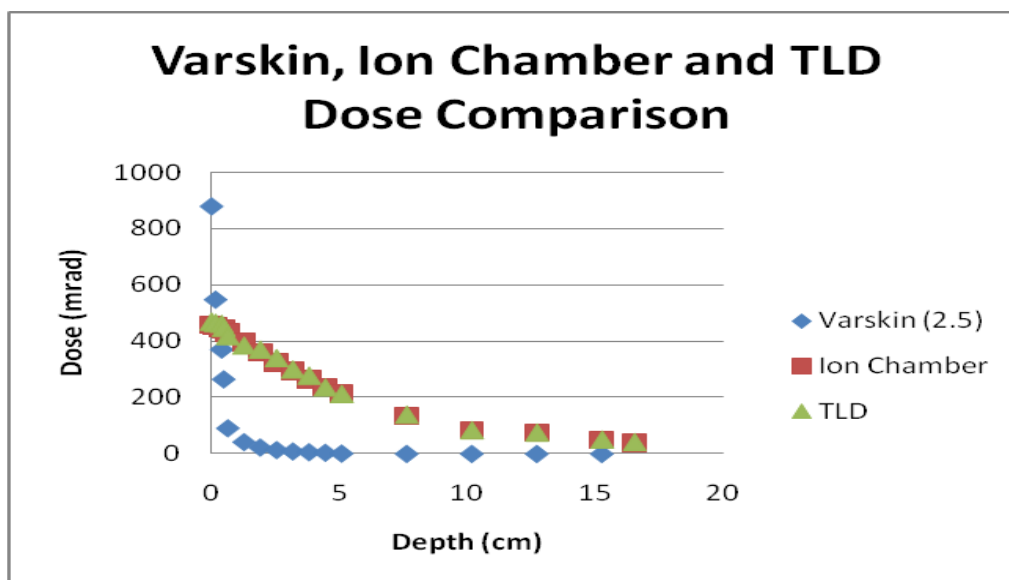


Figure 7-5: Varskin, Ion Chamber and TLD Dose Comparison (2.5 cm^2)

The dose comparison between the VARSKIN 4 program, Ionization chamber, and TLD for a skin averaging area of 2.5 cm^2 (ion chamber) is displayed in Figure 7-6.

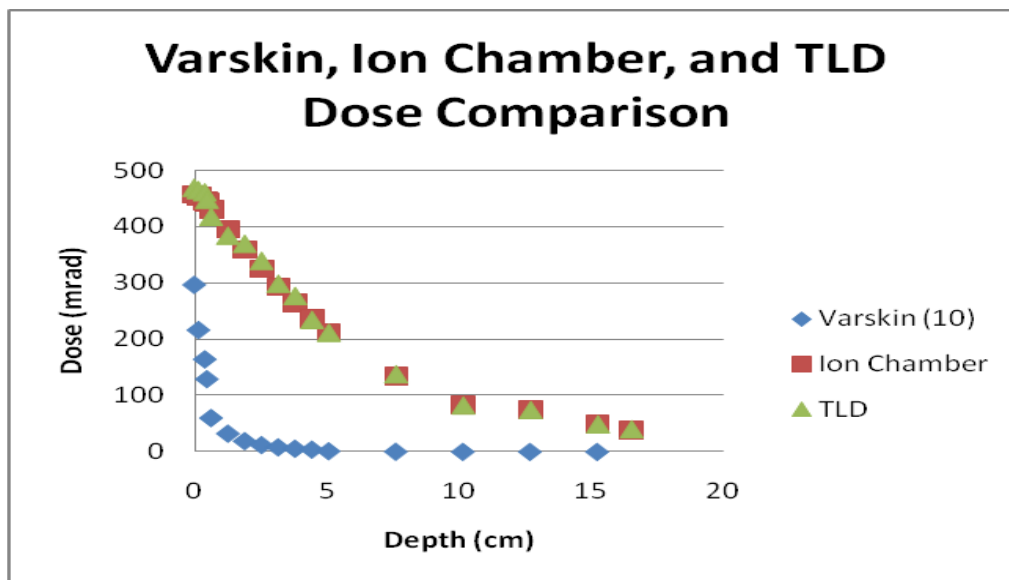


Figure 7-6: Varskin, Ion Chamber, and TLD Dose Comparison

Table 7-4 displays the skin and tissue dose between the VARSKIN program, Ionization chamber, and TLD for a skin averaging area of $.01524 \text{ cm}^2$.

Depth (cm)	Varskin (.01524)(mrad)	Ion Chamber (mrad)	TLD (mrad)
0	9260	457.36	469.09
0.15	7600	453.80	464.77
0.39	1990	445.30	460.93
0.47	876	443.00	447.57
0.63	489	431.00	417.45
1.27	114	395.16	383.71
1.90	47.2	359.46	369.29
2.54	24.7	324.60	338.76
3.17	14.7	292.70	298.18
3.81	9.48	264.10	276.26
4.44	6.47	236.96	233.93
5.08	4.61	211.96	210.86
7.62	1.53	134.40	137.15
10.16	0.64	82.74	81.54
12.70	0.30	74.58	73.38
15.24	0.15	48.89	48.12
16.51	0.01	37.61	39.18

Table 7-4: Dose Comparison Between Varskin, Ion Chamber, and TLD ($.01524 \text{ cm}^2$)

Table 7-5 displays the skin and tissue dose between the VARSKIN program, Ionization chamber, and TLD for a skin averaging area of 2.5 cm².

Depth (cm)	Varskin (2.5) (mrad)	Ion Chamber (mrad)	TLD (mrad)
0	NA	457.36	469.09
0.15	879	453.80	464.77
0.39	548	445.30	460.93
0.47	371	443.00	447.57
0.63	265	431.00	417.45
1.27	91.4	395.16	383.71
1.90	42.2	359.46	369.29
2.54	23.1	324.60	338.76
3.17	14	292.70	298.18
3.81	9.1	264.10	276.26
4.44	6.3	236.96	233.93
5.08	4.5	211.96	210.86
7.62	1.51	134.40	137.15
10.16	0.63	82.74	81.54
12.70	0.30	74.58	73.38
15.24	0.15	48.89	48.12
16.51	0.11	37.61	39.18

Table 7-5: Dose Comparison Between Varskin, Ion Chamber, and TLD (2.5 cm²)

Table 7-6 displays the skin and tissue dose between the VARSKIN program, Ionization chamber, and TLD for a skin averaging area of 10 cm².

Depth (cm)	Varskin (10)(mrad)	Ion Chamber (mrad)	TLD (mrad)
0	NA	457.36	469.09
0.15	296	453.80	464.77
0.39	216	445.30	460.93
0.47	164	443.00	447.57
0.63	129	431.00	417.45
1.27	60.2	395.16	383.71
1.90	32.6	359.46	369.29
2.54	19.4	324.60	338.76
3.17	12.4	292.70	298.18
3.81	8.3	264.10	276.26
4.44	5.8	236.96	233.93
5.08	4.2	211.96	210.86
7.62	1.4	134.40	137.15
10.16	0.62	82.74	81.54
12.70	0.30	74.58	73.38
15.24	0.15	48.89	48.12
16.51	0.11	37.61	39.18

Table 7-6: Dose Comparison Between Varskin, Ion Chamber, and TLD (10 cm²)

The skin and tissue doses for the VARSKIN program do not match the doses from the Ionization chamber or the TLD because of many different factors. The biggest factor is the energy spectrum that the x-ray machine produces which VARSKIN cannot model. The average photon energy of 32 keV that VARSKIN models is not large enough of an energy to penetrate very far into the tissue density. The x-ray machine has a spectrum of energies up to 80 keV which can penetrate all the way through the Plexiglas phantom material.

Another factor is the air gap which VARSKIN is not able to model. VARSKIN can only model an air gap up to 5 cm. The experimental procedure used for the x-ray machine utilizes a 40 inch air gap (source to image distance). Since the air gap cannot

be modeled, the surface dose from VARSKIN does not correlate with the ionization chamber or the TLD and all other absorbed doses do not compare.

The number of bremsstrahlung x-rays produced is another factor which creates the difference in the dose between VARSKIN and the ionization chamber and TLD. Since the number of x-rays produced from an x-ray machine can vary from one machine to another, it is difficult to determine the number of photons striking the detector at any given time. Since there is a spectrum of energies, one cannot determine the number and intensity of each bremsstrahlung photon created when the electrons strike the tungsten target. The differing number and intensity of the x-rays produced will have a great affect on the dose being produced from the x-ray machine to the VARSKIN program. The hand calculation to determine the number of x-rays produced from the x-ray machine is a rough estimate of the true number.

The VARSKIN code was created and developed for use by the NRC staff to calculate skin dose for regulatory requirements. These requirements use a 10 cm² skin averaging area to determine the dose to human skin from a radioactive spill. The program was designed to use the 10 cm² skin averaging area which differs from the thickness of the TLD and the ionization chamber. To set up the VARSKIN program the same as the experimental procedure used on the x-ray machine, it would be optimal to use the thickness of the TLD and the ionization chamber. Since there is no air gap between the skin and the photons, the dose is very large because of the small skin averaging area. The TLD has a thickness of 0.01524 cm² and the ionization chamber has a thickness of 2.5 cm². The small skin averaging areas make the surface dose very large compared to the ionization chamber and the TLD and results in the VARSKIN program not being comparable to an x-ray machine procedure.

The surface dose from the ionization chamber and the TLD's can be used to determine the radiation absorbed dose at different depths within skin and tissue. In practice, a surface dose is measured with a TLD or ionization chamber, and the absorbed dose at any depth in tissue or any other material can be calculated from the

surface dose. By taking the surface dose measurement from the ionization chamber, absorbed doses can be calculated to determine if they correlate with the measured dose from the ionization chamber. Likewise, the surface dose from the TLD can be used to calculate the absorbed dose at any depth within tissue to determine if the measured dose from the TLD is comparable to hand calculations. Figure 7-7 depicts the dose comparison between hand calculations and the ionization chamber.

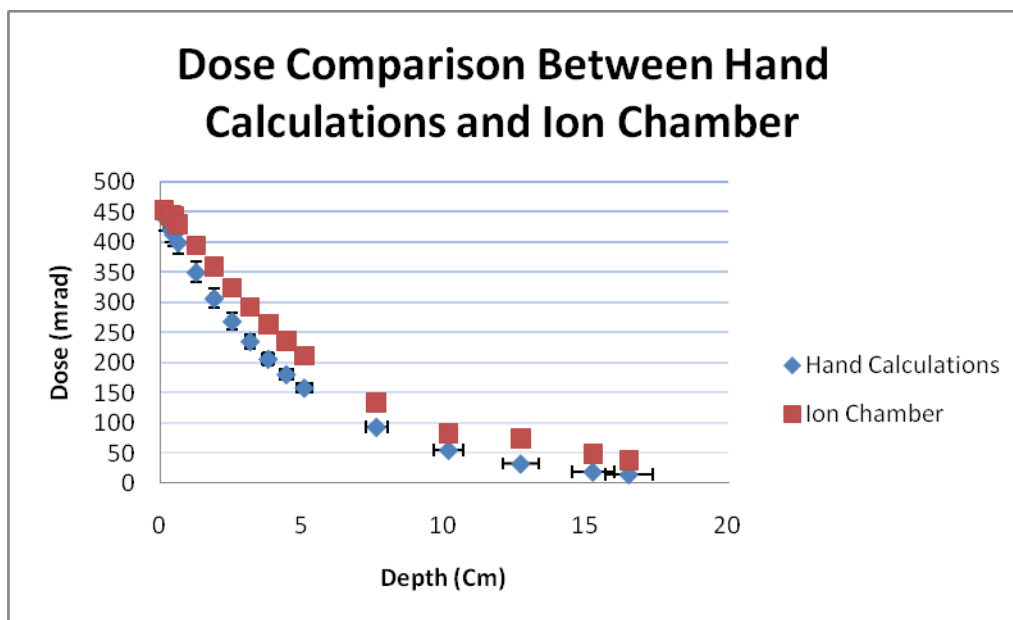


Figure 7-7: Dose Comparison Between Hand Calculations and Ion Chamber

Figure 7-8 depicts the dose comparison between hand calculations and the TLD.

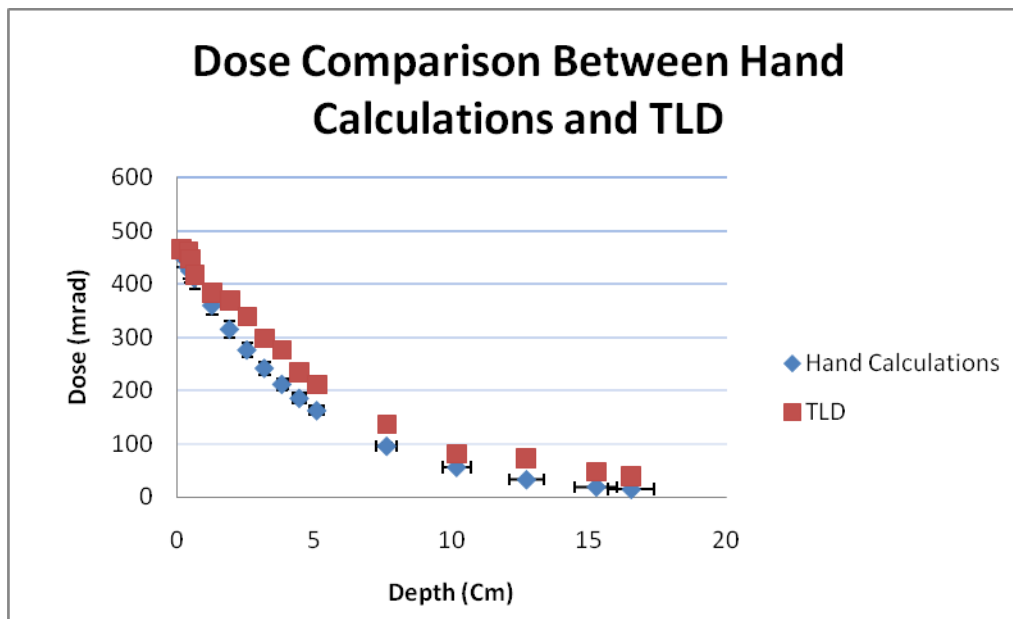


Figure 7-8: Dose Comparison Between Hand Calculations and TLD

Table 7-7 shows the dose comparison and the percent difference between hand calculations and the ionization chamber.

Depth (cm)	Hand Calculations (mrad)	Ion Chamber (mrad)	Percent (%)
0	457.36	457.36	0
0.15	442.49	453.80	2.56%
0.39	421.08	445.30	5.75%
0.47	414.18	443.00	6.96%
0.63	400.71	431.00	7.56%
1.27	351.07	395.16	12.56%
1.90	307.59	359.46	16.86%
2.54	269.49	324.60	20.45%
3.17	236.11	292.70	23.97%
3.81	206.86	264.10	27.67%
4.44	181.24	236.96	30.75%
5.08	158.79	211.96	33.49%
7.62	93.56	134.40	43.65%
10.16	55.13	82.74	50.09%
12.70	32.48	74.58	129.60%
15.24	19.14	48.89	155.44%
16.51	14.69	37.61	156.00%

Table 7-7: Percent Difference of Ion Chamber and Hand Calculations

Table 7-8 shows the dose comparison and the percent difference between hand calculations and the TLD.

Depth (cm)	Hand Calculations (mrad)	TLD (mrad)	Percent (%)
0	469.00	469.00	0
0.15	453.84	464.77	2.41%
0.39	431.88	460.93	6.73%
0.47	424.80	447.57	5.36%
0.63	410.98	417.45	1.57%
1.27	360.08	383.71	6.56%
1.90	315.47	369.29	17.06%
2.54	276.40	338.77	22.57%
3.17	242.16	298.19	23.14%
3.81	212.16	276.26	30.21%
4.44	185.88	233.94	25.85%
5.08	162.86	210.86	29.47%
7.62	95.96	137.15	42.92%
10.16	56.54	81.54	44.21%
12.70	33.32	73.38	120.26%
15.24	19.63	48.12	145.13%
16.51	15.07	39.18	160.02%

Table 7-8: Percent Difference Between TLD and Hand Calculations

8.0 Conclusions

The Ionization chamber and the TLD skin depth dose response at each depth proved to be comparable within five percent. The application of very thin TLD chips for determining dose response at different depths in the skin and tissue was successful despite the inherent statistical variation of the TLDs. The experimental design and procedure was intended to replicate an exact abdominal x-ray procedure to determine if the ionization chamber and the TLD dose response will correspond with skin and tissue depth. Since the doses are within five percent of each other, physicists will be able to utilize the ion chamber and TLD within their calibration testing for surface dose measurements. The calibration testing can also be correlated to a standard x-ray

procedure to establish if the two procedures surface dose measurements are equivalent. This correlation will be helpful in determining if the dose from a standard x-ray procedure is within reasonable range.

By utilizing two detectors for surface dose measurements during calibration testing, physicists can be more accurate within their testing procedures and results because there will be reassurance from two detectors. Even though these instruments are used in different settings, the dose response should be similar so that confidence is gained in terms of potential dose to patients and the control thereof. Since the TLD and ionization chamber have comparable skin depth dose response, physicists will be able to use the two detectors interchangeably within their calibration testing and can monitor and confirm that the calibration testing dose is equivalent to a standard x-ray procedure.

The calibration curve is the most important part of the research when it comes to determining TLD dose. The calibration curve relates a known delivered dose from the TLD output. The pin wheel Radium-226 TLD calibrator is a vital part in calculating and determining the known delivered dose for the calibration curves. This calculation is dependant upon how the radioactive source is modeled and what assumptions are made when modeling. The Radium pin wheel allows the TLD's to have a uniform dose to each TLD Lego because of the circular motion of the wheel. Much attention was given to the modeling process of the TLD's and making sure the TLD's were in the correct location for each set of calibration doses.

If the VARSKIN program proved to be comparable with the TLD and ionization chamber with skin and tissue dose, then physicists could rely on this program to check the accuracy of their testing or to check a patient's dose. Physicists could use this program to check a patient's tissue or skin dose at any depth when a procedure is done and a certain dose to an organ or tissue region needs to be known. VARSKIN would have been a helpful tool for physicists to use to evaluate skin and tissue doses since the program is very easy to use and it only takes a few steps to get results. The

VARSKIN program would have confirmed the accuracy of both the TLD and ionization chamber dose at each depth if the program was able to be modeled after an x-ray machine. Furthermore, VARSKIN has proven that it cannot be modeled after an x-ray machine because of several different variables which make the dose comparison not accurate.

Hand calculations were not accurate with the TLD or the ionization chamber. The percent difference increases as the depth increases and a percent difference of up to one hundred and sixty percent is shown at the bottom of the phantom. In practice, this method is used to determine dose at a certain depth within the skin or tissue. The skin dose was more accurate than the tissue dose but only for the first few skin depths. This type of calculation does not match the ionization chamber or the TLD skin and tissue doses used for an x-ray machine procedure. Since the x-ray machine produces a spectrum of energies, and not a mono-energetic photon, these hand calculations are not accurate. This method is not a reliable way of calculating skin and tissue dose from the surface dose of an x-ray machine and is not comparable to ion chamber or TLD results.

9.0 Future Work

To determine the dose comparability of the ion chamber and the TLD, additional research should be performed on different energy settings on the x-ray machine. The research was performed on a tube potential of 80 kV for both the ion chamber and the TLD to ensure that the experimental design was exact for both detectors. Additional research on a variety of x-ray energies will determine if the ion chamber and TLD dose response to differing skin and tissue depths is truly comparable.

Additional research on the statistical variability of the TLD chips will establish a better conception of the chips characteristics. The calibration curve for the TLD's could contain more data points to increase the accuracy of the linear interpolation of the dose to the experimental TLD's. Each skin and tissue depth contained five

different TLD chips; increasing the number of TLD's per data point would increase the accuracy and statistical variability of the mean TLD output.

Plexiglas was the material used for the phantom which is tissue equivalent. Although Plexiglas is an excellent tissue equivalent material, there are several other materials which are tissue equivalent and used for calibration testing. Utilizing a few different phantom materials will determine if the ion chamber and the TLD are truly comparable. The different tissue equivalent material could perhaps result in different doses at skin and tissue depths between the ion chamber and the TLD. Using a variety of phantom material will confirm that the ion chamber and the TLD are comparable with skin and tissue depth.

Along with different tissue equivalent material, additional research could be done using a different ionization chamber and a different vendor for the TLD's. Having different experimental equipment will determine the exact dose comparison between the ion chamber and the TLD.

If the VARSKIN program made changes in the future to add a larger air gap between the source and the skin surface, additional research could be done to verify that VARSKIN could be in fact comparable to the ion chamber and TLD dose from an x-ray machine. The air gap parameter, along with the energy spectrum of the x-ray machine, were the biggest factors in the doses not being comparable to the ion chamber and the TLD.

10.0 Bibliography

- 23391, 5. F. (1991). *10CFR20: Energy, Standards for Protection Against Radiation*. Nuclear Regulatory Commission . Office of the Federal Register.
- A.D.A.M. A.D.A.M. Interactive Anatomy Online. Retrieved from <http://adameducation.com>
- Adnani, N. (2006). *Entrance Skin Dose Using Dose-Area Product Measurements: Application to a Cardiac Catheterization Laboratory*. McKee Cancer Center.
- Bacci, C. (1993). *Contact Radiotherapy Machine Calibration by Means of TLDs*. Radiation Protection Dosimetry (Vol.47 No.1/4).
- Bakshi, A.K. (2009). *Energy Response study for Thermoluminescent Dosimeters to Synchrotron Radiation in the Energy Range 10-35 keV*. Indian Journal of Engineering & Materials Sciences.
- Balter, Stephen. (2010). *Fluoroscopically Guided Interventional Procedures: A Review of Radiation Effects on Patients Skin and Hair*. Radiology (Vol.254 No.2)
- Brock, K. M. Oregon State University Radiation Center Health Physics Procedures (2001). *RCHPP 15: Operating Procedures for the Environmental Thermoluminescent Dosimetry (TLD) Program*.
- Carron, N.J. (2007). *An Introduction to the Passage of Energetic Particles through Matter*. New York: Taylor & Francis Group.
- Cazalas, E. "Design, Construction, and Analysis of a Skin Contamination Dosimeter". Master's Thesis. November 2009.
- Cember, H., T. E. Johnson (2009). *Introduction to Health Physics*. New York: McGraw Hill.
- Fraser, Danielle. (2009). *Characterization of Cylindrical Ionization Chamber for Patient Specific IMRT QA*. Journal of Applied Clinical Medical Physics (Vol. 10 No.4).
- Gad, Shani (1991) *Radiation Dosimetry: Instrumentation and Methods*. Ann Arbor: CRC Press.
- Goffman, J.W. (2000). *Do X-ray Practitioners Give Enough Attention to Minimizing the Patients' X-ray Dosage?* The X-ray and Health Project. The Committee for Nuclear Responsibility.
- Hazle, John D. (1992). *Quality Assurance of Intra-operative Electron Radiotherapy Clinical Trials: ionization Chamber and Mailable Thermo-luminescent Dosimeter Results*. International Journal of Radiation Oncology Biology Physics. Volume 24. Issue 3.
- Health Physics Society (2010). Retrieved from hps.org

- Hendee, W.R. (2002). *Medical Imaging Physics* (4th Ed.). Wiley-Liss, Inc.
- Hobbs, T. (1996). *Response Comparison of Electret Ion Chambers, LiF TLD, and HPIC*. Radiation Protection Dosimetry. Oxford Journals.
- International Commission on Radiological Protection. (1991). *ICRP 59: The Biological Basis for Dose Limitation in the Skin* (Vol.22 No.2) Oxford: Pergamon Press.
- Khan, F.M. (2003). *The Physics of Radiation Therapy* (3rd Ed.). Lippincott Williams & Wilkins
- Kinhikar, R. (2008). Phantom Dosimetric Study of Nondivergent Aluminum Tissue Compensator using Ion Chamber, TLD, and Gafchromic Film. *Medical Dosimetry*. Volum 33. Issue 4.
- Kinhikar, R. (2007). *Intensity Modulated Radiotherapy Dosimetry with Ion Chambers, TLD, MOSFET, and EDR2 Film*. Australian Physical and Engineering Sciences in Medicine. Vol. 30 Number 1, 2007
- Knoll, G. F. (2000). *Radiation Detection and Measurement* (3rd Ed). Hoboken, NJ: John Wiley & Sons, Inc.
- Lindell, Bo. *International Commission on Radiological Protection: History, Policies, Procedures*. Swedish Radiation Protection Institute.
- Martin, C.J. (1998). *Protocol for Measurement of Patient Entrance Surface Dose Rates for Fluoroscopy X-ray Equipment*. The British Journal of Radiology.
- Martin, J. E. (2006). *Physics for Radiation Protection* (2nd Ed). Wiley-VCH.
- Martini, M.H. (2006). *Fundamentals of Anatomy and Physiology* (7th Ed). Pearson-Benjamin Cummings.
- McMaster Carr. (2009). Retrieved from <http://www.mcmaster.com>
- National Council on Radiation Protection and Measurements. (1999). NCRP Report No. 130: Biological Effects and Exposure Limits for Hot Particles. Bethesda, MD.
- National Council on Radiation Protection and Measurement. (2004). NCRP Statement No. 10: Recent Applications of the NCRP Public Dose Limit Recommendation for Ionizing Radiation. Bethesda, MD.
- National Nuclear Data Center. Chart of the Nuclides. Retrieved from Brookhaven National Laboratory: <http://www.nndc.bnl.gov/char/>

Peet, D.J. (1999). *Evaluation of a MOSFET Radiation Sensor for the Measurement of Entrance Surface Dose in Diagnostic Radiology*. The British Journal of Radiology.

Sedecal. (2010). Retrieved from <http://sedecal.com>

Shultis, Kenneth J., Richard E. Faw, Fundamentals of Nuclear Science and Engineering. New York: Marcel Dekker, Inc., 2002.

ThermoFisher. (2010) Retrieved from <http://thermofisher.com>

Keizer, K. (2010) "Performance Validation of a Prototype Skin Contamination Detector via Use of Very Thin Thermoluminescent Dosimetry". Master's Thesis.

Stanton, L. Day. (1999). *Comparison of Ion Chamber and TLD Dosimetry in Mammography*. Pubmed.gov

Turner, J. E. (2007). *Atoms, Radiation, and Radiation Protection* (3rd Ed). Wiley-VCH.

Varksin 3: A Computer Code for Assessing Skin Dose from Skin Dose Contamination. Center for Nuclear Waste Regulatory Analyses. U.S. Nuclear Regulatory Commission Office of Nuclear Regulatory Research, Washington D.C. October 2006

